Advances in Applied Energy 3 (2021) 100046

Contents lists available at ScienceDirect

Advances in Applied Energy

journal homepage: www.elsevier.com/locate/adapen

# Urban cells: Extending the energy hub concept to facilitate sector and spatial coupling

A.T.D. Perera [a,b,*], Kavan Javanroodi [c], Y. Wang [d], Tianzhen Hong [a]

[a] Building Technology and Urban Systems Division, Lawrence Berkeley National Laboratory, 1 Cyclotron Road, Berkeley, CA, 94720, United States
[b] Urban Energy Systems Laboratory, EMPA, Überland Str. 129, 8600 Dübendorf, Switzerland
[c] Solar Energy and Building Physics Laboratory (LESO-PB), Ecole Polytechnique Fédérale de Lausanne (EPFL), CH-1015 Lausanne, Switzerland
[d] Institute of Thermal Science and Technology, Shandong University, Jinan, China

ARTICLE INFO

*Keywords:*
Distributed generation
Sector coupling
Multi-agent systems
Urban cells
Interconnected energy infrastructure
Urban systems

ABSTRACT

The rapid growth of urban areas and concerns over climate change make it vital to improve the energy sustainability of cities. Understanding the complex interactions within different sectors (sectoral) and localities (spatial) of cities plays a crucial role in improving efficiency and sustainability, which is extremely challenging due to the complex urban morphology. State-of-the-art energy concepts do not facilitate a detailed consideration of both sectoral and spatial coupling that energy infrastructure maintains at the urban scale. This has become a significant challenge when designing interconnected urban energy infrastructure. The Urban Cell concept is introduced to address this bottleneck. A novel computational model using a modular approach is introduced to create an interconnected urban infrastructure, including the energy, building, and transportation sectors. Optimal sizing of the distributed energy system (including renewables, energy storage, and dispatchable sources) and optimal urban morphology is determined within a modular unit. A game-theoretic approach is used to model the interactions between urban cells (modular units). The study revealed that the urban cell concept can reduce the net present value of the interconnected energy infrastructure by 37% while increasing the installed renewable energy capacity by 25%. This demonstrates the benefit potential of urban cells and the importance of considering interactions between different sectors and different parts within a city. The Urban Cell concept can be used to present the complex interactions maintained within a city.

## 1. Introduction

Cities are growing rapidly, and it is expected that 68% of the global population will live in cities by 2050 [1]. Empirical research suggests densification as an approach to stop expanding urban infrastructures and higher demand for mobility [2]. Urban densification can result in a more complicated urban morphology [3], leading to a convoluted urban climate due to urban heat island (UHI) effects [4]. Densification also can lead to higher energy use in cities, and consequently, higher demand for resources. Already 80% of energy is consumed within cities, and that consumption is responsible for 60% of anthropogenic carbon dioxide ($CO_2$) emissions. Densified urban areas can accelerate this upward trend by modifying the amount of solar radiation [5,6], shading [7,8], and heat transfer from external surfaces [9,10]. It also can alter indoor thermal comfort conditions [11] and, accordingly, increase cooling and heating demand [12,13] and lighting electricity consumption [14]. Therefore, it is necessary to develop urban areas more sustainably, as defined by the United Nations Climate action sustainable development goal (SDG 13).

Climate adaptation of urban energy systems includes improving sustainability. Renewable energy integration and improving the efficiency of building stock play a vital role in improving sustainability. Certain urban forms increase renewable energy integration and reduce heating and cooling energy demands [15,16]. Therefore, the urban planning process can notably influence the energy transition in urban infrastructure. However, very few studies have focused on this particular aspect, despite its timely importance. Similar to the building sector, climate change and air quality problems in urban areas will require sustainability improvements in the transportation sector by extensively promoting electric vehicles (EV) and EV charging infrastructure. Large-scale adoption of EVs, especially in mixed-use urban areas, introduces a large amount of time-varying charging demands to the network. Integrating energy demand for EV charging into buildings can alter building performance and energy consumption profiles [17]. The impacts of EV

* Corresponding author.
*E-mail address:* atperera@lbl.gov (A.T.D. Perera).

https://doi.org/10.1016/j.adapen.2021.100046
Received 19 March 2021; Received in revised form 5 June 2021; Accepted 13 June 2021
Available online 23 June 2021

charging on building performance and load profiles have not been assessed comprehensively [18] at the urban scale. This could lead to inconsistencies in urban planning, resulting in impaired reliability and renewable energy integration of the urban energy system [19].

Several concepts have recently emerged in the energy sector to support the energy transition. The smart grid concept was introduced to enable a more interactive grid, moving away from the existing classical grid architecture with a hierarchical setup and unidirectional power flow to facilitate large-scale integration of renewable energy technologies [20]. Maintaining interoperability within the electricity sector was a primary objective focus when introducing the smart grid concept. Often the operation and stability of the grid are the focus, with few studies focused on the design aspect. The concepts of the fourth and fifth generations of district heating networks were introduced into the heating sector to develop a smart thermal grid with objectives similar to those of the electricity sector [21]. Similarly, several advancements have been made within the energy system domain. The concept of hybrid energy systems has been introduced to integrate renewable energy technologies into distributed generation (often discussed in off-grid applications) [22]. The concept of energy hubs has been introduced as an extension to hybrid energy systems, considering multiple energy services such as electricity, heating, and cooling [23]. However, studies of the interlinks between these distributed energy hubs and network models have been limited, therefore we lack a deep understanding of its magnitude and the spatial and temporal patterns that arise when moving into an urban scale.

Interactions between distributed energy systems located at different localities within a city (spatial coupling) play a vital role at the urban scale. Distributed energy systems can help each other withstand the fluctuations in both demand and generation, which will improve renewable energy utilization while minimizing operation costs [24]. Facilitating such interactions while maintaining security is a challenging task [25]. Besides interacting with neighboring energy systems at the urban scale, energy systems are expected to interact locally with the building and transportation sectors (sector coupling) [26]. Interactions maintained locally between different sectors help improve energy systems' flexibility, which plays a pivotal role in improving the renewable energy penetration levels. More important, existing concepts within the energy system domain do not facilitate consideration of such complex interactions maintained within the urban context, making it difficult to design interconnected urban energy infrastructure. Therefore, it is necessary to address the following research questions to shape the energy transition and improve sustainability in urban areas:

1 How should the energy hub concept be extended to facilitate both spatial and sector coupling?
2 How should the existing bottom-up design models be extended to consider spatial and sector coupling to design interconnected infrastructure?
3 What is the best way to facilitate the autonomy of each sector at different geo-spatial scales while developing integrated infrastructure (especially in security/privacy and data sharing)?

Addressing these challenges is essential to improve sustainability in cities where a conceptual intervention is essential. As a means of addressing these research problems, Section 2 introduces the concept of the *Urban Cells*. A modular architecture is presented in Section 3 to design integrated urban cells. The optimal design of each distributed energy system (determining the optimal component sizes for photovoltaic [PV] panels, wind turbines, energy storage, combined heat and power generation [CHP] units, and heat pumps) and urban morphology (urban form and urban density, considering the electric transportation) are considered at the module level. A game-theoretic framework is introduced to reflect the spatial coupling between the modular units while preserving privacy. Section 4 illustrates a case study. Finally, Section 5 presents the impact of considering sector and spatial coupling and benchmarks the present concept against the novel methodology introduced in the study.

## 2. Urban cells

Consideration of the urban context requires energy system models to be substantially extended to consider other infrastructures such as buildings, transportation, and water distribution. Several concepts enable consideration of the energy nexus with transportation and water. The first part of this section provides a holistic background on the energy nexus in an urban context and the limitations in the present state of the art, mostly related to the energy hub concept. The second part presents the novel approach.

### *2.1. Background*

Linking multiple sectors and several localities within a city demands a detailed information flow. Existing computational tools do not facilitate such a detailed workflow that covers different sectors and localities. Therefore, customized workflows that combine several computational tools are often used. The energy nexus with transportation, buildings, water distribution, and purification has been addressed using such customized workflows. For example, many studies have comprehensively investigated the integration of e-mobility into existing energy systems and related demand response potential, including smart charging and vehicle-to-grid systems. However, the impacts of e-mobility integration on energy system design are often overlooked. Few studies consider EV charging demand when sizing the capacity of various conversion and storage technologies for energy supply systems. Cao et al. [27] considered EV charging demand in a sizing problem of mixed conversion technologies (i.e., fuel cells, CHP, gas boilers, and PV) for a multi-energy system. Murray et al. [28] optimized the size, configuration, and operation of a multi-energy system considering both building and EV energy demands and compared the competitiveness of different EV technologies on decarbonizing the community in future scenarios. Murray et al. [29] optimally selected vehicle technologies, including internal combustion engine vehicles and EVs, along with building system technologies for urban energy system design. These studies provide insights into how EV charging demand affects the energy system design process, which can be further extended by linking the building sector. EV charging demands show distinct characteristics concerning land-use types, which is often considered in the deployment problems of EV charging [30]. However, linking the EV charging process has not been considered together with the urban planning and energy system designing process, where both sector and spatial coupling play a vital role.

Several research studies have attempted to develop workflows that combine numerous computational tools and platforms [31,32] to analyze the complex energy flows within urban areas, taking into account the urban morphology. For example, Mohajeri et al. [33] studied the sensitivity of urban form to integrated PV electricity generation, renewable energy integration, and grid price from 2017 to 2050, considering two major urban development strategies (densification and expansion). Nonetheless, most of these studies are limited to a single urban neighborhood. The complex interactions between different neighborhoods at an urban scale are ignored in the procedure. The unidirectional flow of information is considered from both transportation and building energy models towards the energy system model, which does not reflect the reality. The scalability of these workflows beyond one distributed system has not been tested. Furthermore, the flexibility of the workflows to accommodate more sectors is doubtful, as most of the workflows are specific and cannot be generalized. The brief literature review reflects that the current practice of using workflows fails to present the complex interactions that take place within cities. This situation demands that we move beyond workflows and establish a generalized model that facilitates sector coupling that can be extended to an urban scale.

### 2.2. Present state-of-the-art concepts for urban systems

Several concepts have been introduced to facilitate energy transition in the urban context. For example, the smart grid was introduced to move towards a more interactive grid. The energy hub model is introduced to facilitate multiple energy conversions within energy systems, improving renewable energy penetration while catering to multiple energy services such as heating, electricity, cooling, and more. Industry ecology is one of the most widely used metaphors in urban systems. The basic thinking behind industrial ecology is also shared by the studies of *urban metabolism,* which is defined as the sum of the technical and socioeconomic processes in cities, resulting in growth, energy production, and waste elimination. Both energy system and energy hub concepts were limited to the energy sector. In contrast, industrial ecology and urban metabolism have not been applied along with urban energy systems models. These models do not facilitate a bottom-up approach when accommodating interactions within different parts of the cities. As a result, it is challenging to use models developed based on these concepts directly to consider both sector and spatial coupling. Therefore, it is essential to extend present concepts related to the energy sector to enable the design of integrated urban infrastructure that efficiently interacts with other sectors and facilitates renewable energy technology integration. The urban cellular architecture is introduced in this study to address this research gap.

### 2.3. Urban cell as a unit to represent sector coupling

A number of energy and mass conversion processes occur within a neighborhood, facilitating many services. Usually, these services are classified into different sectors to make the analysis simple. In general, heating, cooling, and electricity supply in buildings are considered to be building services. Similarly, cities also have energy services, transportation services, and other types of services, and often these service sectors interact with each other. Urban Cell is used to consider these interactions within a neighborhood. Within this context, a city is divided into several metropolitan districts, and each urban district has multiple cells at the neighborhood level (Fig. 1). Each cell can be regarded as a multifunction unit with several system layers, representing sectors such as buildings, energy, transportation, and industry (Fig. 1(e)). The system configuration (design) of each layer depends on the services provided by the sector and its interaction with the other system layers. For example, a cell with a dense urban morphology (i.e., a complicated building system layer) will require a higher energy demand for electricity, heating, etc. (larger capacity in the energy system layer). In addition, the configuration of the system layers depends on the local conditions and the system layers of the neighboring cells. Design optimization of a cell determines the optimal system configuration for each system layer, and that is the main focus of this study. For example, for the energy system layer, design involves optimal sizing of renewable energy technologies, energy storage, dispatchable sources such as combined heat and power generators, energy conversion devices (heat pumps and chillers), and other factors. Similarly, for the building system layer, design involves determining the optimal building form and building density. The objective of the cell is to improve the autonomy of the neighborhood while enhancing the efficiency of the interactions maintained between the different sectors within the neighborhood.

### 2.4. Urban cellular networks

While the urban cell facilitates the interactions between different sectors, inter-cell interactions enable spatial coupling. Therefore, interactions between urban cells play a vital role in utilizing the resources. Networks that maintain connectivity between different parts of a city play a crucial role in this regard. Thermal, gas, electricity, and road networks are some examples in this regard. Connectivity between the cells enables the grid to withstand the imbalances of generation and demand for services. The multiplex network between the cells facilitates interactions between the cells within certain flow constraints, allowing them to accommodate the fluctuations. The cells operate autonomously as agents, which formulates a multi-agent network problem. Therefore, the urban cellular network (UCN) concept converts the urban system design problem into a distributed multi-agent design problem.

Multi-agent network problems have been amply discussed from the control system perspective, especially with reinforcement learning intervention [34]. Multi-agent models have been used to represent the possible operation modes of distributed microgrids and communication systems being aligned with control theory [24]. Nonetheless, to the best of the authors' knowledge, it has not been used for urban system design. Two operation modes can be defined as being aligned with the control system community: fully cooperative scenarios and non-cooperative scenarios. A *fully cooperative* scenario explains the operation of a multi-agent system with centralized intervention. The operation states of all the systems are shared, or a centralized authority intervenes when determining the actions. The security of operating agents becomes a significant concern. However, a detailed understanding of the entire distributed system enables one to reach optimal solutions with a better performance. In contrast, *non-cooperative* systems do not share information in such a manner. Agents compete with each other and the competition enables them to determine an optimal strategy to maximize their performance. The non-cooperative approach performs better to protect privacy, although the performance of the system can be notably poor compared to the cooperative scenario. The study proposes a *leader-follower* strategy to take advantage of both cooperative and non-cooperative scenarios. The leader-follower approach enables UCNs to operate efficiently while preserving privacy. Each cell shares certain information with the leader (e.g., time series grid injection, grid purchase), which helps to determine the connectivity among the cells. Each cell determines its system design on its own based on the network constraints to interact with the neighboring cells.

## 3. Methodology

Bringing several sectors together is a challenging task. As shown in Fig. 2, a clear workflow is developed to achieve this objective, making it easy to understand the energy, material, and cash flows in between sectors. The workflow begins with an understanding of the energy requirements for the building sector. Energy demand for heating, cooling, and electricity depends on the urban morphology. Further, the energy demand depends on the type of building, e.g., residential, industrial. The building energy demand of the cell is computed considering both these aspects. A detailed explanation of the methodology used to calculate the building energy demand is explained in Section 3.1. Similarly, urban morphology is the starting point when determining the EV energy demand. Depending upon the urban morphology, the maximum number of occupants is obtained. Based on the maximum number of occupants, building function, and occupancy profile it is possible to determine the energy demand for EVs and requirements for charging stations for an urban cell, as explained in Section 3.2. Finally, the energy system is optimized considering the energy demand for buildings and transportation, as described in Section 3.3. The optimal set of designs for each cell are fed into the secondary level optimization, which uses a game-theoretic approach to determine the optimal design for each urban cell and the connecting energy network, as explained in Section 3.4.

### 3.1. Generating urban cell models and energy simulations

The current state-of-the-art modeling urban morphology can be divided into two major approaches: real case studies [35] and idealized urban areas [36]. Several studies have linked morphological parameters with energy demand in terms of urban form (density [10], the geometry of the buildings [37], building envelop [38]), urban structure (streets

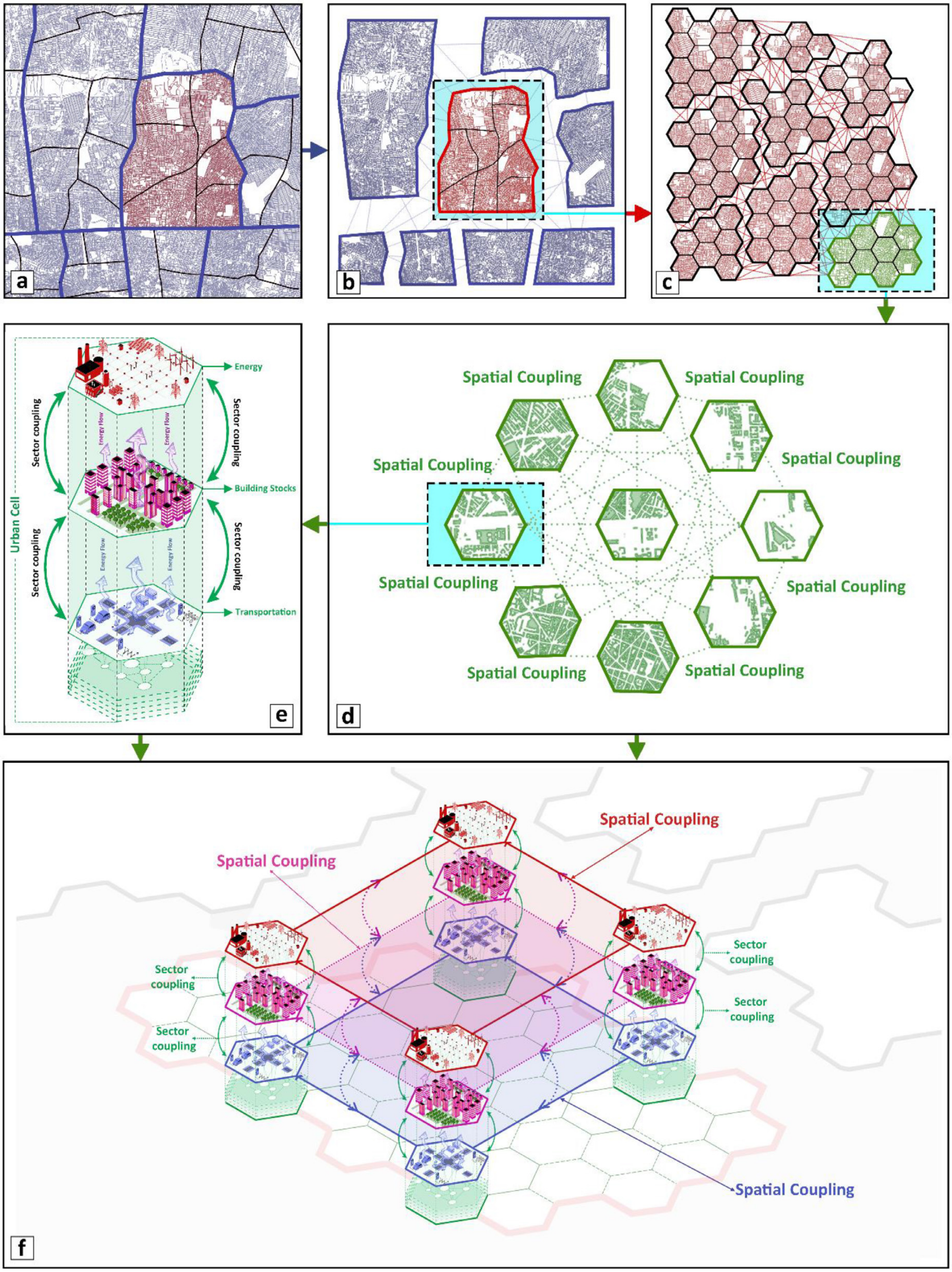


**Fig. 1.** The overview of the urban cell concept is presented in Fig. 1. The urban area taken for the study is presented in 1(a), which consists of several districts as presented in 1(b). A district consists of several urban cells which (1(c)) interacts with each other enabling spatial coupling (1(d)). Each urban cell consists of several layers, as presented in 1 (e), where each layer represents a particular sector (such as energy, building, etc.). Urban cells facilitate interactions between these layers, enabling sector coupling (1(e)). This formulation helps the urban cell concept facilitate spatial and sector coupling, as shown in 1(f), which helps design complex interconnected urban infrastructure.

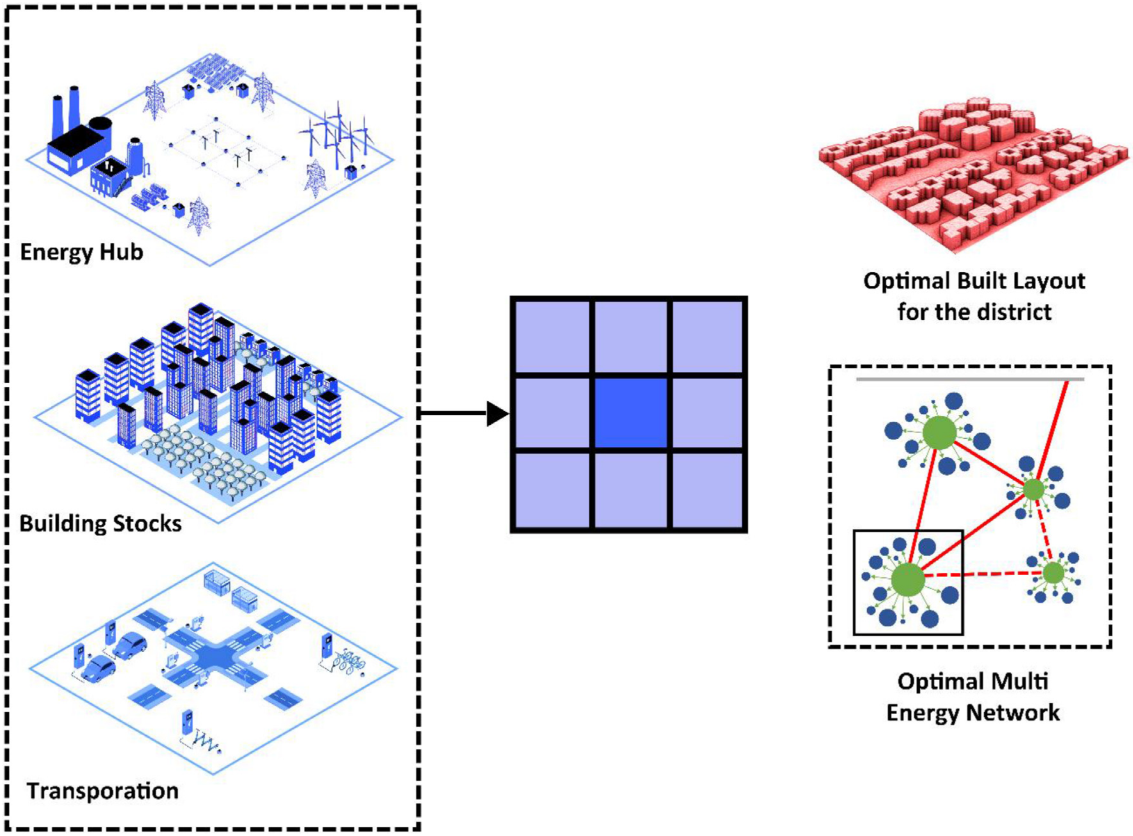


**Fig. 2.** The workflow illustrating the novel design approach presented in this study for interconnected energy infrastructure. The city is divided into several cells. Sector coupling between energy, building, and transportation sectors is considered for each cell. Subsequently, the spatial coupling between different cells is considered.

and sidewalks [39], as well as the distance between buildings [40]), and urban function (operation of buildings [41] and open spaces [40]). However, the existing urban building energy models mostly focus on one specific urban neighborhood and fail to consider complex interactions among several urban neighborhoods, which is essential to design an urban cell. Thus, to capture the interactions between several sectors in an urban cell, a series of urban neighborhoods need to be modeled based on realistic morphological parameters.

This study adopted and further developed a method, namely *Building Modular Cell* or *BMC,* introduced by Javanroodi et al. [42]. BMC is based on a cuboid module (4 × 4 × 4 m) that considers the main influencing morphological parameters to generate complex urban models. Here, a set of nine urban neighborhoods (each with 208 × 208 m dimensions) were designed as a matrix with three rows and columns. Three main categories were considered to define the distance between neighborhoods and buildings located at each neighborhood, including highways (width = 40 m), streets (width = 12 to 16 m), and canopies (width=6 to 8 m). Each urban neighborhood consisted of four areas with 96 × 96 m dimensions (total area of 9216 $m^2$s [$m^2$]). The designed urban cell had 704 × 704 m dimensions (total area of 495,616 $m^2$) with four main building types: stand-alone houses (RE-SA), multi-family apartments (RE-MF), small offices buildings (OF-S), and large office buildings (OF-L).

The central neighborhood was considered to be the district center, with large office buildings and a large green space (96 × 96 m), while the rest were divided into four main areas. Based on the building types, each area consisted of 12, 9, 4 subsites for RE-SA (144 subsites), RE-MF (108 subsites), and OF-S building types (32 subsites), respectively, which resulted in 296 distinct subsites in the designed urban cell. To design the building layout in each subsite, four main morphological parameters were considered as design constraints; these included: Plot Area Ratio (PAR), Volume Area Ratio (VAR), Site Coverage Index (SCI), and Building Height Index (BHI) (Fig. 3). For example, neighborhood 6 (N6) had a constraint of 58.3, 34%, 41%, and 282 for PAR, VAR, SCI, and BHI, respectively (Fig. 3-b).

By defining these parameters for each subsite, area, neighborhood, and urban cell, a total of 296 building layouts were designed. For RE-SA, RE-MF, OF-S, and OF-L a total number of 6, 8, 9, and 3 distinct architectural layouts were used to generate 296 buildings in the urban cell. Two major design constraints based on SCI and Building Height Density (BHD) were used to design each building. For SCI, a built density constraint of 50%, 60%, 70%, and 80% was used for RE-SA, RE-MF, OF-S, and OF-L buildings. For BHD, a series of height constraints were assigned to each building type: RE-SA (2 floors), RE-MF (4, 6, 8 floors), OF-S (12, 18, 20 floors), and OF-L (24 floors). The window-to-wall ratios (WWR) were also assigned based on the building types. The WWR of residential buildings was 18%, 35%, 12%, and 12% for the northern, southern, western, and eastern sides, respectively, while these values were 12%, 25%, 8%, and 8% for office buildings.

The detailed urban cell model (Fig. 4) was generated by a Grasshopper script and exported to EnergyPlus through Diva for Rhino 4.0. Each module was designed as a thermal zone; the number of thermal zones is dependent on the PAR and VAR parameters of each building type. The cooling/heating demand, equipment, and lighting energy demand profiles were calculated for all thermal zones at each floor of building blocks as the combination of latent and sensible loads. To account for the impact of UHI effects, the Dragonfly plugin from Ladybug tools [43] was adopted (see Section 4: Application case studies for more details on the adopted weather data). Furthermore, the impacts of the surrounding buildings for each building are also considered through the true view

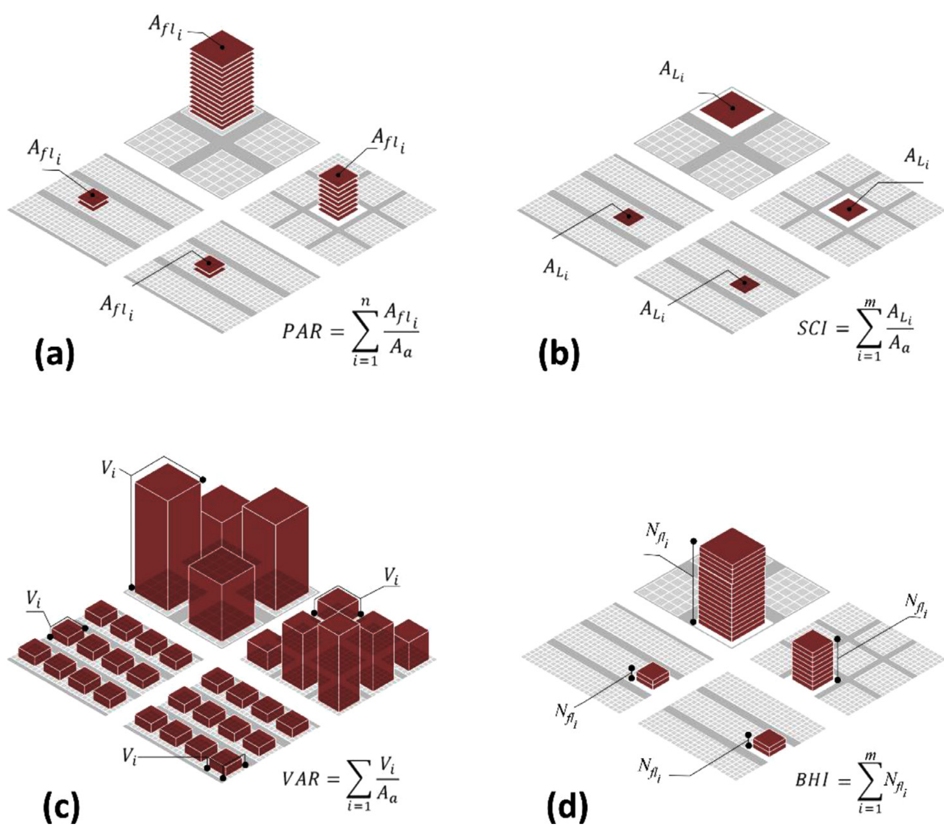


**Fig. 3.** Adopted morphological parameters to design the urban cell and its components: (a) Plot Area Ratio (PAR): the total area of all floors divided by the total area of the site, (b) Site Coverage Index (SCI): the total area of the ground floor divided by the total area of the (sub) site, (c) Volume Area Ratio (VAR): the total volume of the buildings divided by the total area of the site, and (d) Building Height Index (BHI): the total number of building floors per each (sub) site.

**Table 1**
Details of EV penetration and distribution.

| Neighborhood | Type | Total Number of Occupants | Total Number of EVs |
|---|---|---|---|
| 1 | RE-SA, & RE-MF | 370 | 51 |
| 2 | OF-S (2688) | 2864 | 373 |
| | RE-SA, & RE-MF (170) | | 25 |
| 3 | RE-SA, & RE-MF | 396 | 55 |
| 4 | OF-S (2688) | 2914 | 373 |
| | RE-SA, & RE-MF (226) | | 31 |
| 5 | OF-L | 1097 | 153 |
| 6 | OF-S (2688) | 2913 | 373 |
| | RE-SA, & RE-MF (225) | | 31 |
| 7 | RE-SA, & RE-MF | 370 | 51 |
| 8 | OF-S (2688) | 2914 | 373 |
| | RE-SA, & RE-MF (226) | | 31 |
| 9 | RE-SA, & RE-MF | 396 | 55 |
| Sum | 14,234 | 1975 | |

factor algorithm in EnergyPlus, by affecting direct/diffuse solar radiation beam networks. The total heat transfer through external surfaces (wall, roof, floors, and windows)—as well as internal loads (e.g., people density, equipment, and lighting) and infiltration through the building envelope and openings—were defined based on the function of each building. The modeling and simulation of urban morphologies with governing equations have been thoroughly described and verified in previous studies [42,44,45].

### 3.2. Modeling the electric vehicle fleet energy demand

EV model is used to compute the charging demand of vehicle fleet depending upon the urban morphology considered. The ownership of cars in Sweden is 555 cars per 1000 people. The EV penetration is assumed to be 25% [46]. In this study, the penetration of EVs in different neighborhoods was determined by occupant density, as tabulated in Table 1.

Localizing EV charging demand to neighborhoods within urban areas has been an important step towards effective planning of electric vehicle supply equipment (EVSE) and relevant energy systems. Unlike petrol-based vehicle drivers, EV drivers tend to keep a relatively high battery level due to range anxiety and connect EVs to the grid whenever possible. According to EV usage statistics, 20% of charging events take place in public locations. In addition, private EVSE is installed at home [47]. In anticipation of the popularization of charging infrastructure, it is assumed that EVs will be connected to the grid during parking periods. In this case, the EV charging demand highly depends on the battery use of previous trips.

In the existing literature, charging demand modeling is usually fulfilled under the assumption that EVs only charge once at certain locations, i.e., home or workplace. The current methods generally lack the capacity to represent different characteristics of EV charging demand concerning different building types, which is essential when designing urban cells. Therefore, this paper adopts an agent-based trip

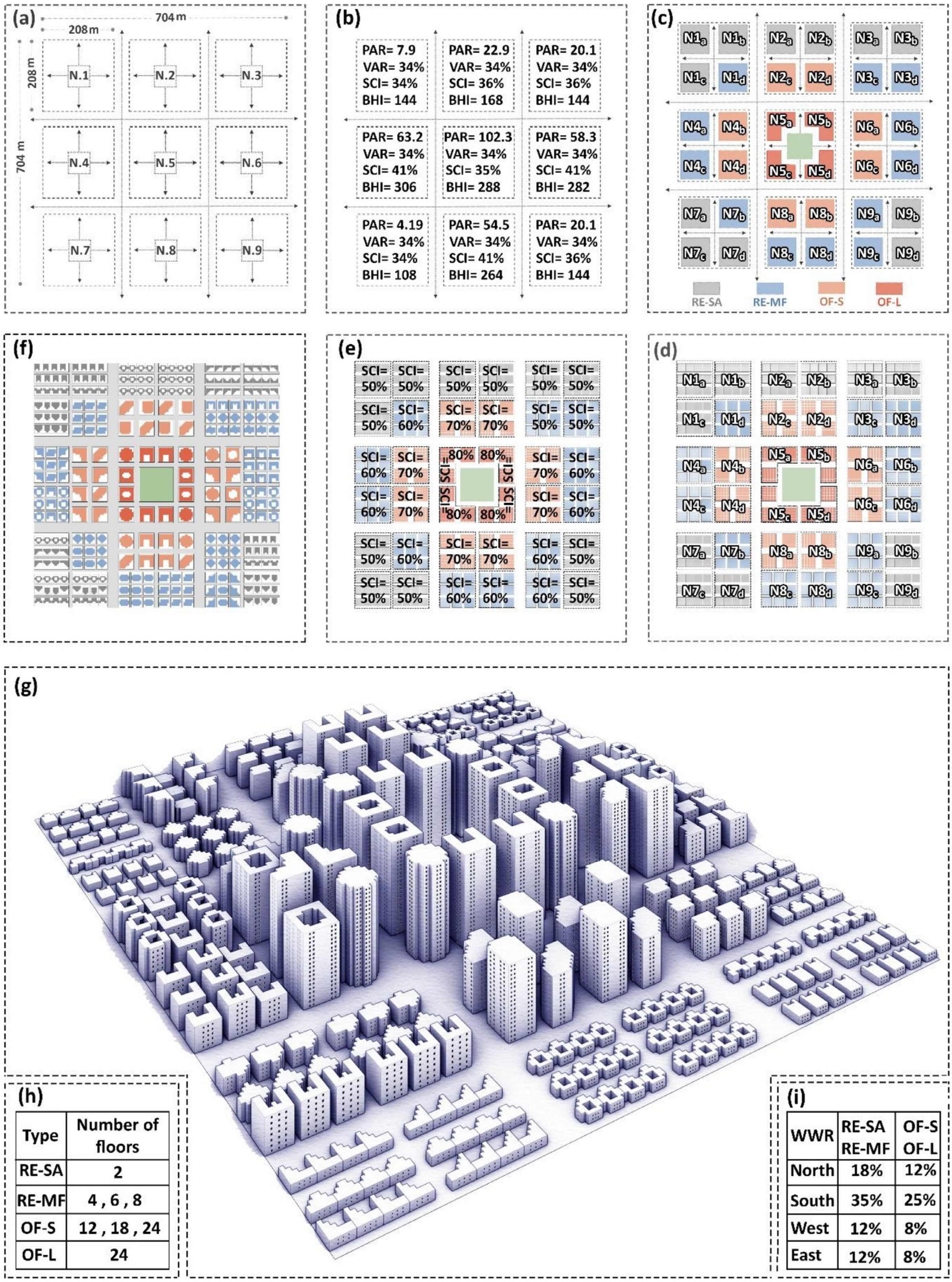


**Fig. 4.** The procedure to design and generate the urban cell including the urban neighborhoods, areas, and subsites (SCI and BHI are used for each neighborhood, and each subsite; PAR and VAR are only used to define neighborhoods). (a) the dimensions and number of 9 neighborhoods, (b) defined values for the main influencing morphological parameters for each neighborhood, (c) urban areas in each neighborhood based on the building types, (d) 296 subsites in all the urban areas based on the building types, (e) site coverage for each subsite in each urban area based on the building types, (f) 296 building layouts with 26 distinct architectural designs based on each building type, (g) the 3D model of the urban cell considering PAR, VAR, SCI, and HBI parameters, (h) the number of floors based on each building type, and (i) WWR values based on the façade directions and building types.

chain model (ABTCM) to represent the relation between building forms and EV charging demand.

The ABTCM generates a full loop of daily trips for each EV agent and parameterizes each trip with six parameters: departure place, departure time, driving distance, driving time, destination, and parking time. The mathematical description of the trip chain vector is presented by Eq. (1)–(3). The values of the parameters vary with the hour of the day and land-use types of the departure place and the destination. Three types of land use are recognized in ABTCM: residential, working, and public locations. The charging demand at residential and working areas is localized to residential and office buildings.

$$\begin{aligned}&\left(p_{d,1}, p_e, T_{d,1}, t_d, t_p, d_d\right)\\&= \left(p_{d,1}; p_{e,1}p_{e,2}\ldots p_{e,m}; T_{d,1}; t_{d,1}, t_{d,2}\ldots t_{d,m}; d_{d,1}, d_{d,2}\ldots d_{d,m}\right)\end{aligned} \tag{1}$$

$$p_{d,m+1} = p_{e,m},\ m = 1, 2, 3\ldots \tag{2}$$

$$T_{d,m+1} = T_{d,m} + t_{d,m} + t_{p,m}, m = 1, 2, 3\ldots \tag{3}$$

where $m$ represents the index of the trip; $p_d$ and $T_d$ represent the departure place and time, respectively; $d_d$ and $t_d$ represent the driving distance and time, respectively; $p_e$ represents the destination, and $t_p$ represents the parking time at the destination $p_e$.

The probability density functions of the trip chain parameters are extracted from real-world vehicle travel data and could represent the realistic temporal and spatial distribution of EV charging demand. The state of charge (SOC) of the EV battery is calculated by Eq. (4) and (5). The energy consumption of a trip is assumed to be in proportion to the driving distance. The charging power of the EVSE is assumed to have three levels: 3.3 kW (kW), 6.6 kW, and 44 kW. EVs tend to charge at the 3.3 kW level unless the parking time is too short (i.e., less than half an hour) or they cannot charge enough electricity to satisfy the next trip.

$$SOC_{t+1} = SOC_t - \frac{a\, E\, d_{d,m}}{C} + \frac{b\ P_{C,t}\ \Delta t}{C}, \tag{4}$$

$$a, b = \begin{cases} a = 1,\ b = o,\ when\ EV\ is\ driving \\ a = 0,\ b = 1,\ when\ EV\ is\ charging \\ a = 0,\ b = 0,\ when\ EV\ is\ neither\ charging\ nor\ driving \end{cases} \tag{5}$$

where $t$ is the index of time step; $SOC$ represents the state of charge of EV battery; $a$ and $b$ are binary parameters that represent the state of EV; $E$ is the electricity consumption per kilometer; $C$ represents the capacity of EV battery; $P_c$ represents charging power, and $\Delta t$ represents the duration of a time step.

### 3.3. Computational model for each cell

Each cell consists of an energy system, which caters to the energy demand for the building sector and the EV's energy demand. The energy demand of the cell depends on the urban morphology, which influences the energy demand for both the building and transportation sectors. The distributed energy system considered in this study consists of renewable energy technologies such as building-integrated PV, wind turbines, a dispatchable energy source, and energy storage interacting with the grid. Heat pumps cater to the energy demand for heating. Grid curtailments were introduced on an hourly basis for both injecting and purchasing electricity to and from the grid based on the congestion of the entire network determined when optimizing the network layout between the urban cells.

The energy system model takes time-series data for renewable energy generation potential, energy demand, and meteorological data for hourly simulations. Also, techno-economic data such as component efficiencies and installation and operation costs were taken as inputs to the model. A time-series simulation was performed to identify the mismatch between renewable energy generation and the energy demand, leading to quantifying energy storage requirements, a dispatchable energy source, and grid interactions. Hourly solar irradiation (global horizontal) and wind speed (at wind turbine hub level) were used as the inputs to the model used to compute the renewable energy generation. Renewable power generation from the PV panels and wind turbines was calculated using Eq. (6).

$$P_t^{RE} = G_t^{\beta}\eta_t^{PV} A^{PV} x^{PV} \zeta^{PV} + \tilde{P}_t^{W}\left(\mathrm{v_t}\right)x^{\mathrm{w}}\zeta^{w}, \forall t \in T \tag{6}$$

In this equation, $G_t^{\beta}$ and $\eta_t^{PV}$ present the global solar irradiation on the tilted PV panel and the efficiency of the PV panel computed by using the Durisch model [48]. Similarly, $\tilde{P}_t^{W}(\mathrm{v_t})$ presents the power generation from a single wind turbine. The number of PV panels and wind turbines within the system is presented by $x^{pv}$ and $x^{\mathrm{w}}$ . The surface area of the solar panel is presented by $A^{PV}$. Complexities brought by the cities make it challenging to consider shading, especially when performing energy system sizing. We introduced a shading factor, $\varsigma^{PV}$, to account for the losses due to shading. Similarly, wind speed will be dropped due to the urban boundary layer. The losses in power converters are presented by$\varsigma^{w}$ in the system and the power losses. Dispatchable source and grid and energy storage cater to the mismatch between renewable power generation and multi-energy demand. The optimal capacity for the dispatchable source and the storage was determined by the optimization algorithm based on the objective function values obtained from the lifecycle simulation of the energy system.

Optimal operation of the dispatchable energy sources, energy storage, and grid interactions depend on many factors, including the mismatch between energy demand and renewable energy generation, grid curtailments, and electricity cost in the grid. Dispatch strategy helps to determine the optimal operation state for dispatchable source, energy storage, and grid interactions. There are different techniques to figure out the optimal operation strategy. For example, dispatch strategies based on reinforcement-learning techniques can present a complex dispatch strategy [49] that can accommodate complex interactions such as demand response strategies [34]. However, training such complex learning techniques demands extensive computation, which becomes demanding with a game-theoretic optimization process. Therefore, a relatively simple dispatch strategy introduced by Perera et al. [56] was used in the present work. The dispatch strategy consists of two levels, where operating conditions of the dispatchable sources (ICG (internal combustion generators)) are determined at the primary level by taking into account the mismatch between energy demand and renewable energy generation, state of charge in the battery bank, and price of electricity in the grid. The interactions between energy storage and the grid are determined at the secondary level, where finite-state theory is used. A more comprehensive definition of the state space of the dispatch strategy is presented in [50].

### 3.4. Design optimization for the urban cell

Design optimization at the urban cell is performed to provide an optimal set of design alternatives to be considered when optimizing the entire UCN. Two objective functions are considered in this regard: the net present value of the system and the grid integration level, which align with the previous work by Wang and Perera [24,25] to optimize Robust Energy Internets. The robust operation requirement in the network guaranteeing n-1 security is not considered in this work, since optimizing the UCN is computationally extensive compared to a simple energy internet.

The urban cell's net present value is determined considering lifecycle cash flows for the energy system and the EV station. Cash flow requirements for the building construction and operation are not considered. The net present value (NPV) of the design represents the financial feasibility. NPV consists of the initial capital cost (ICC) and operation and maintenance (OM) costs of the energy system and EV charging center. For example, installation costs involving acquiring and installing PV panels, wind turbines, etc. are considered under ICC. OM consists of two components: (1) fixed operation and maintenance cost$OM_{c,s}^{Fixed}$ and (2) variable operation and maintenance costs ($OM_c^{\text{variable}}$). Charges related to regular maintenance functions are considered under the $OM_{c,s}^{Fixed}$. $OM_c^{\text{variable}}$ presents variable OM related to the replacement of system components such as a battery bank. The NPV of the urban cell is computed according to Eq. (7).

$$NPV = ICC + \sum_{\forall c \in C} (OM_{c,s}^{Fixed} CRF_c) + \sum_{\forall h \in H} \sum_{\forall c \in C} PRI^l OM_{c,h,s}^{\text{variable}}, \quad \forall t \in T, \forall c \in C, \forall h \in H \tag{7}$$

In Eq. (7), $CRF_c$ denotes the capital recovery factor for the c$^{\text{th}}$ component. *PRI* denotes the real interest rate calculated using both interest rates for investment and the local market annual inflation ratio. The year considered is represented by *h*.

Grid integration level brings a different perspective, which represents the autonomy level. Lower grid integration levels will lead to a higher autonomy level. Grid integration level is defined in this study according to Eq. (8) [51].

$$GI = \sum_{\forall t \in T} E_t^{IG} / \sum_{\forall t \in T} E_t^D \tag{8}$$

In this equation, $E_t^{IG}$ and $E_t^D$denote energy imported from the grid and energy demand of the hub. A steady $\varepsilon$-state evolutionary algorithm is used in this study to obtain the Pareto solutions, and it is based on the $\varepsilon$-dominance method [52].

### 3.5. Design optimization for the cellular network

The optimal solutions obtained by optimizing distributed urban cells provide sets of alternative design solutions, which need to be considered for the optimal urban cellular network. Besides obtaining the optimal urban cellular design at each cell, it is necessary to optimize the connectivity among the urban cells. The optimal design for the network and the urban cell are closely interlinked. The close connectivity between these two formulates a complex objective function, neither linear nor convex, making it difficult to optimize both these sectors simultaneously. The approach used in this study to address this issue is based on the previous work of Wang and Perera [24,25], where a similar interactive system solely considering the energy sector is worked out. Besides moving into the building and transport sector, the study uses a non-cooperative leader-follower strategy different from the fully cooperative strategy proposed by Perera and Wang [25]. The non-cooperative architecture provides more flexibility and autonomy to the urban cells, which is essential when designing such distributed systems coupling multiple sectors. The optimization of the cellular network begins with optimizing each urban cell considering preset limits for network interactions. Subsequently, both connectivity of the network and optimal design for each urban cell are selected at the secondary level. The results of the secondary level are used to update the grid curtailments, which will be used for the optimization of the urban cell. The optimization process is conducted iteratively until the results converge.

The secondary level optimization is performed considering two objective functions: (1) the net present value of the entire UCN and (2) the autonomy of the UCN. The net present value of the UCN is computed considering the net present value of all the urban cells, installation, and the operation and maintenance cost for the distributed network (Eq. (9)).

$$NPV_{ESPG/FCS}^{IE} = \sum_{\forall h \in H} NPV^h + \sum_{\forall l,m \in H} NPV^{x_{lm}} \tag{9}$$

In Eq. (9), $x_{lm}$denotes the installation, operation, and maintenance cost for the line connecting energy hub $l$ and $m$. $NPV^h$ indicates the net present value of a system installed in an urban cell. The decision space consists of urban cell design p$^{\text{h}}$ ($p\forall \in P^h, \forall h \in H$) for each cell and connectivity strength for$x_{lm}(x\forall \in X)$.

Grid interactions maintained with the transmission network (IT) are computed similarly. Both selling and purchasing are minimized for the UCN. Eq. (10) is used to compute the IT.

$$IT = \frac{\sum_{\forall t \in T} P_t^{IG,EI} + P_t^{EX,EI}}{\sum_{\forall h \in H} \sum_{\forall t \in T} P_{t,h}^{ELD}} \tag{10}$$

The optimization process consists of several steps, as presented in Fig. 5.

**Step 1:** The optimal configuration of the urban cell is obtained considering energy system configuration, urban morphology, and the electricity demand for EV. The energy demand of the building stock and EV charging, wind, and solar energy potential is considered on an hourly basis for each cell during the optimization. A set of Pareto solutions are obtained considering Net Present Value and the grid interactions of the cell as presented in Eq. (7) and 8. Loss of load probability within the grid was set to be as less than 0,1% within the cell during the optimization (introduced as a constraint). In addition, injection and purchasing electricity from the grid is maintained within the capacity bounds of the grid which vary on the network optimization performed in Step 3. The cells having higher NPV will depend less on the grid while the cells having lower NPV will depend more on the grid connecting the cells. An evolutionary algorithm is used in this study to arrive at the Pareto front. For readers who are interested in further details about the formulation of the objective functions and methodology used for the optimization can go through Ref. [50,51,53].

**Step 2**: Following Step 1, Pareto solutions are obtained which presents a unique urban morphology (along with an EV profile matching into the urban morphology), energy system configuration. This stage is devoted to organizing the Pareto solutions obtained in Step 1 in a manner that these Pareto solutions can be used in Step 3 when optimizing the energy network. Pareto solutions are organized in descending NPV order for each urban cell. A decision vector is used in each urban cell to consider the Pareto solutions organized. Each Pareto solution within the urban cell will have a unique pattern of grid injection and purchase of energy which is considered in Step 3. The optimal decision vector value for each urban cell is obtained in Step 3 along with the network optimization problem.

**Step 3:** The first stage of Step 3 is devoted to optimizing the network configuration connecting the urban cells and the decision vector that presents the configuration of the urban cell (as described in Step 2). The Transportation model introduced by Romero et al. [54], is used to evaluate the network flow. The flow model is subsequently extended following the formulation presented in [24,25] to support the optimization of the network. Wang and Perera et-al. [25] uses a bi-level optimization algorithm for Step 2. In the study of Wang and Perera et-al. [25], primary level of the optimization algorithm uses Particle Swarm Algorithm (PSA), which use to optimize the system configuration while the second level uses mixed integer linear programing technique to optimize the network. The present study moves beyond the energy system by considering urban morphology and the transportation sector which makes it difficult to use the mixed integer linear programming formulation. Therefore, a heuristic algorithm is used in this study to optimize both urban configuration and network. In the present study, the Pareto sets determined by Step 1 is used as the input to Step 2. Each energy system consisting of a set of alternative solutions as explained in Step 2. The strength of the network, as well as system configuration for each hub, is optimized in Step 3. After completing the optimization process, flexibility of each line in the network is computed on hourly basis which is used to derive the injection and purchase limit for each urban cell.

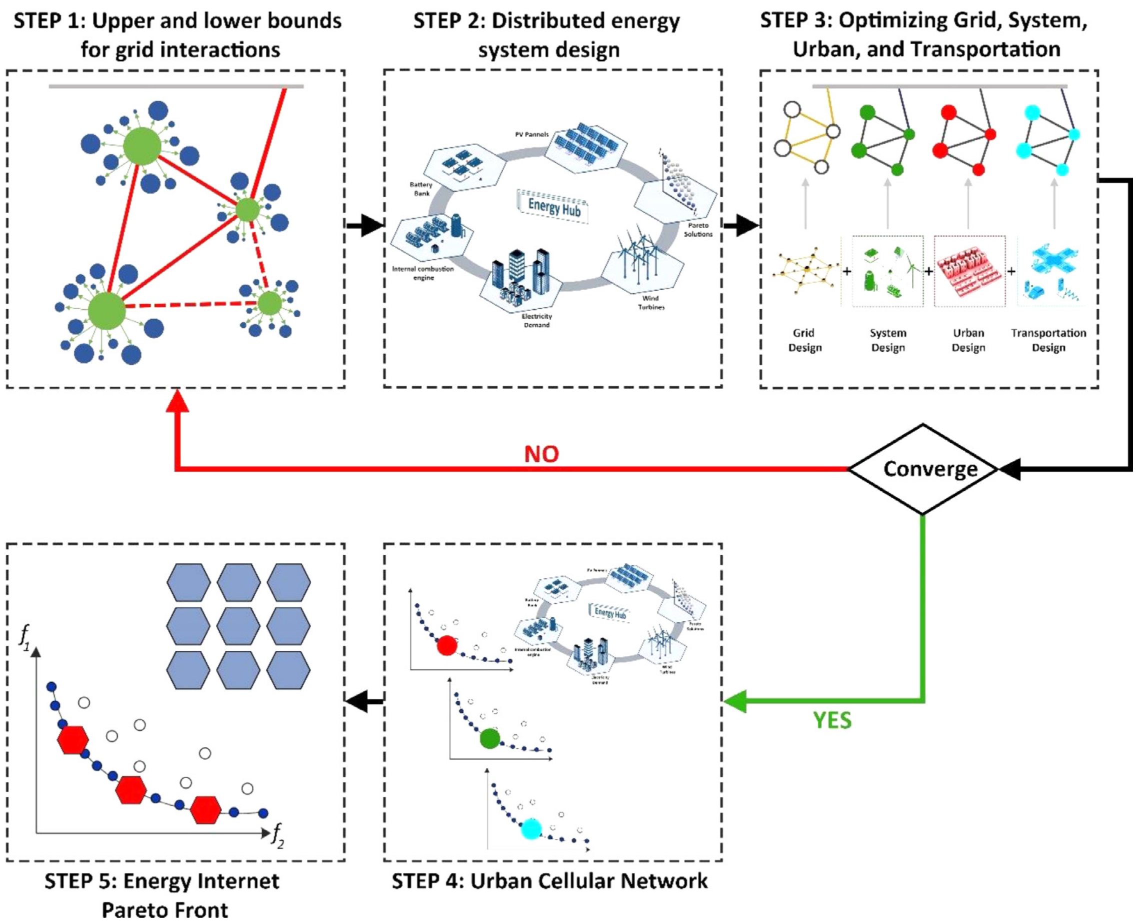


**Fig. 5.** Optimization framework to link urban energy system.

**Table 2**
Benchmark scenarios for comparison.

| | Scalable Interconnectivity | Sector Coupling |
|---|---|---|
| Urban Cellular Network | Considers | Considers |
| Isolated Coupled Infrastructure | Not considered | Considers |
| Fixed Generation Scenario | Not considered | Not considered |

**Steps 4 and 5:** The steps explained in 1, 2, and 3 are performed in an iterative manner until we reach the epsilon Nash equilibrium. After reaching the epsilon Nash equilibrium the optimal urban cell configuration is obtained in Step 4 and the optimal network connection between the urban cells is obtained in Step 5.

The urban morphology and electric vehicle fleet have a notable impact on the energy demand profile. To evaluate the effectiveness of UCNs, we used two benchmark scenarios. The first was the Fixed Generation Scenario (FGS), where urban morphology is fixed and merely the energy generation system is optimized, taking predefined grid curtailments. FGS considers neither sector coupling nor spatial coupling. The second scenario was Isolated Coupled Infrastructure (ICI), where each cell is optimized considering predefined network capacities (without considering the network interactions). Therefore, the iterative procedure updating the grid and energy system design was not performed in this scenario. These two scenarios were used to benchmark two interesting characteristics of urban cellular networks: sector coupling and scalable interconnectivity (Table 2). Subsequently, both FGS and ICI were compared with UCNs to evaluate the impact of the novel concept.

## 4. Application case study

The Capital city of Stockholm (latitude: 59.3 N, longitude: 18.06 E), as the most populated city in Sweden, was selected as the case study. Stockholm is located on fifteen islands on Sweden's east coast, and it has 11 municipal districts and a total area of more than 118 square kilometers (km$^2$) [55]. The city is experiencing a dramatically high expansion rate and a construction boom to tackle the rapid population. As a result, several interconnected complex geometric urban forms, ranging from dense city centers to detached buildings, have been built during the last four decades [56]. The city has a moderate continental climate with cold winters and mild summers. The average air temperature in January is between −4 °C and 0 °C; it is 11 °C to 20 °C in June. To consider the impact of urban microclimate conditions on the weather data, the Dragonfly plugin [43] (as a component of the Ladybug Tools plugin in Grasshopper) was adopted based on the Urban Weather Generator (UWG) tool [57]. It is well known that the roof shape of buildings can affect both microclimate conditions [58], its indoor air quality [59], and energy performance [60]. In this study, based on morphological parameters of the newly-built urban areas in Stockholm, flat-form roofs were assigned to the buildings. The typical meteorological year (TMY) weather file for Stockholm Arlanda Airport was adopted and morphed using the Dragonfly plugin from Ladybug tools [43] to account for urban heat island effects in the simulations. In this regard, each building was defined as an obstacle considering its type (e.g., residential, office). For vegetation, the designed green space in the central neighborhood was also connected to the Dragonfly plugin. The major outputs of the Dragonfly plugin (e.g., dry-bulb and dewpoint temperature, wind speed, relative humidity, direct/diffuse radiation) were extracted to conduct the morphing process. Then, the morphed weather data were used to run annual simulations for cooling and heating demands, as well as for electricity demand (equipment and lighting) for all defined thermal zones.

In the Swedish transportation sector, about 4.8 million passenger cars were registered in 2017 [61]. By 2019, private cars contributed a total of 6.7 billion miles of vehicle mileage [62]. In anticipation of an increasing number of EVs and plug-in hybrid EVs (PHEVs) in Sweden, 20% of vehicle mileage contributed by private cars will be satisfied with electricity; the number of EVs and PHEVs will reach 1 million by 2030 [63]. In this paper, the realistic travel patterns were extracted from the American National Household Travel Survey (NHTS) database to generate the ABTCM. The source data, along with validation, can be found in [64]. The values were scaled down to agree with the annual vehicle mileage of Swedish passenger cars, which is 1171 miles [62].

## 5. Results and discussion

The design of each cell may have a unique energy system design that caters to the building stock requirements, vehicle charging is considered for each cell. Cells interact with each other through the support of energy networks. Joint optimization of each cell can lead to an improvement in the overall efficiency within the UCN. However, a qualitative analysis will help reveal the widespread influence of urban morphology and EV energy demand on the energy infrastructure. The first part of this section presents a comprehensive assessment of energy demand for all the cellular archetypes used in this study, considering transportation and building energy. The second part is devoted to optimizing UCNs. Scenarios consisting of four, six, and nine cells were considered, to evaluate the impact of the novel concept to improve the renewable energy integration level and minimize operation cost.

### 5.1. Impact of urban morphology on the energy demand

This section presents the results of energy simulations based on the defined morphological parameters. Fig. 6 illustrates the cumulative distributions of hourly heating and cooling demands per square meter for all nine urban neighborhoods. The peak heating demand per square meter occurred in N5 with large-scale offices (3.07 kWh/$m^{-2}$). Apparently, the heating and cooling demand per square meter in N5 was notably higher than in the rest of the neighborhoods due to building type. This value in other neighborhoods was 96% higher than N1, N3, and N9, while it was 64%, 52%, 56%, and 57% higher than N2, N4, N6, and N8, respectively. The standard deviation difference in N5 compared to N1, N3, and N9 was more than 94%. This high standard deviation in the neighborhoods with office buildings was due to the working hours plan (8 a.m to 5 p.m.).

To better convey the impacts of urban morphology, the daily and monthly energy demand (the sum of heating and cooling) and appliance demand per square meter for three neighborhoods with mixed-building types is shown in Fig. 7. The average energy demand in the office-dominant neighborhood was about 0.16 kWh.$m^{-2}$ which is about 76% and 63% higher than those of N3 and N8, respectively. The highest energy demand in the office buildings was seen from 7 a.m. to 9 am (Fig 7. a). This is due to working schedule in office buildings, where HVAC is turned off during nights and higher energy is required during mornings to reach indoor thermal comfort condition. In contrast, for residential buildings, higher energy demand was seen at night with higher occupancy density. In terms of appliances, demand (equipment and lighting), the main variations can be seen in the lighting demand (Fig 7. b). For residential buildings (N1), the highest appliances demand can be seen during nighttime (7–10 pm). The N8 with small office buildings showed lower lighting demand than large-scale office buildings (N5) due to higher vertical density and, accordingly, a higher amount of shading. It is important to see the monthly demand profiles of urban neighborhoods in relation to local climate region (Fig 7. c). As the designed urban cell is located in a cold climate zone (Stockholm), heating demand is considerably larger than cooling demand. A similar demand pattern can be seen in all three neighborhoods, whereas the highest and lowest monthly energy demand happens in January (e.g. 234 kWh.$m^2$ in N5) and July (e.g. 23.2 kWh.$m^2$ in N5) under the impacts of temperature variations. On the contrary, the appliances energy demand does not vary significantly in respect with seasonal variation. The difference between appliances energy demand in January and July is less than +1%, +7% and +4% for N1, N5, N8 respectively; where larger lighting demand is required in months with higher could cover.

To provide an insight into other elements of urban morphology, the performance of buildings with similar functions needs to be assessed. Fig. 8 illustrates annual energy demand in kWh.$m^{-2}$ for similar building types with similar built density and heights in N1, N2, N7, and N8. In stand-alone residential buildings (N1 and N7), the average energy demand during winter in N7 was notably (up to 50%) higher than it was in N1. A closer look shows that buildings with a courtyard form had a higher heating demand, while showing a better performance during warm months. It is interesting to mention that buildings with similar built forms showed a lower annual average and peak energy demand in N1 due to urban form. One reason is a lower amount of shading during cold months in N1 with fewer high-rise obstacles. A similar trend can be seen in the multi-family residential building (N1 and N8), with about 18% annual average and 49% higher peak demand in N8 due to higher shadings. In the case of small-scale office buildings in N8 and N2, U-form buildings showed less than 5% lower demand than C-form buildings. On the other hand, for buildings with similar forms and characteristics, the energy demand difference between N8 and N2 is less than 7% on the annual average. A trend can be noticed in buildings with a higher number of floors (final height of the buildings), where the impacts of urban morphology on energy demand decrease notably. The building floors located higher than the regular urban canopy layer showed lower sensitivity to the microclimate variations. These complex interactions between multiple neighborhoods can introduce large impacts on the energy system performance indicators.

Another aspect of assessment is quantifying the impacts of interconnectivity on the energy performance of a generated UCN. Three different scenarios were defined for this purpose, including UCN A (nine neighborhoods), UCN B (six neighborhoods: N4, 5, 6, 7, 8, and 9), and UCN C (four neighborhoods: N2, 4, 6, and 8). Fig. 9 compares annual energy demand in kWh.$m^{-2}$ for each scenario. An overview of the results clearly shows the impacts of interconnectivity, where a higher number of considered neighborhoods resulted in lower energy demand per square meter. The UCN C scenario had the highest average energy demand (0.09 kWh.$m^{-2}$), compared to UCN A and B with 27% and 6%, respectively. The impacts can be seen in peak energy demand, where UCN C (1.33 kWh.$m^{-2}$) showed 25% and 6% higher magnitude compared to UCN A and UCN B. These impacts can introduce up to a 25% variation, which can be critical in designing energy systems.

### 5.2. Impact of urban morphology on electricity demand

The normalized electricity demand of appliances in three neighborhoods with mixed-building types is presented in Fig. 10. For each neighborhood, the hourly values of appliance demand were averaged over the one-year simulation results based on weekdays and weekends. In a neighborhood dominated by residential building (N3), electricity demand showed a similar pattern on weekdays and weekends, and showed clear daily peaks and valleys in their daily electricity usage. N5, the office-dominated neighborhood, showed the highest normalized electricity demand on weekdays among all neighborhoods and the lowest on weekends. For N8, which has both small office buildings and residential buildings, the electricity demand patterns combined in N3 and N8.

Another important aspect of the assessment is to look into the impacts of urban morphology on the EV charging demand profiles. Elec-

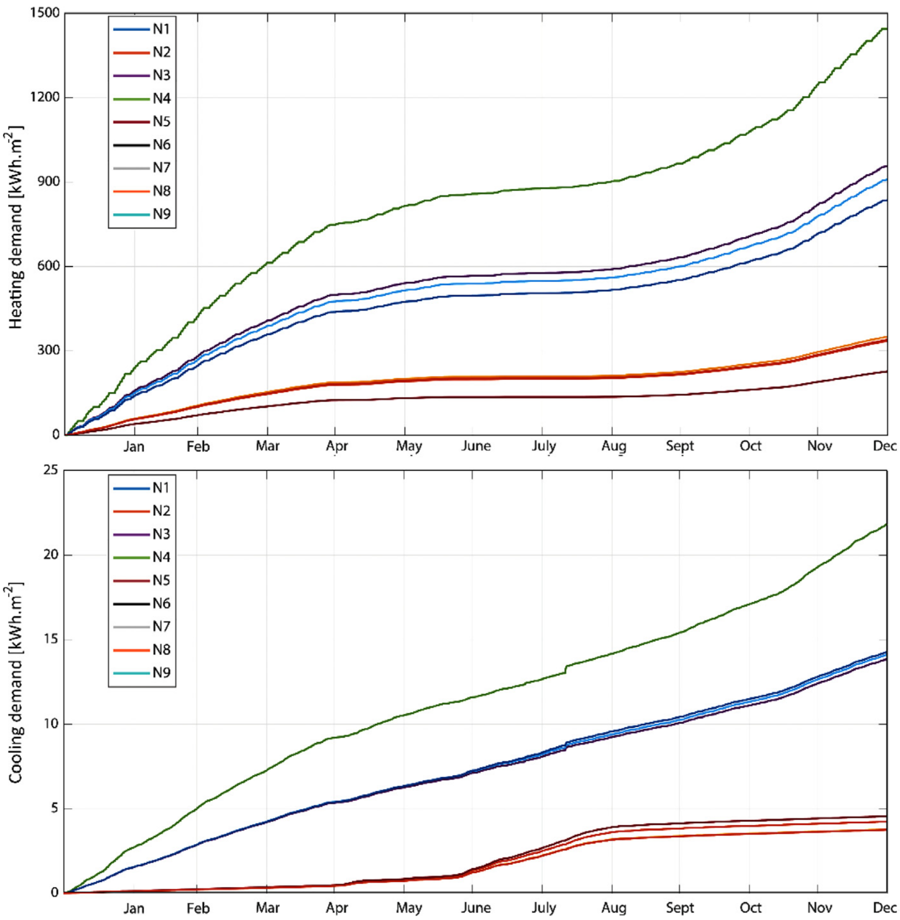


**Fig. 6.** Cumulative heating (top) and cooling (bottom) demand for all neighborhoods in the urban cell.

tric vehicle charging patterns are affected by the EV owners' behaviors and thus showed different characteristics in different types of buildings. Fig. 11 shows the average charging demand per EV for N3, N5, and N8 on weekdays and weekends. Similar to the appliance demand, the derived EV charging demand profiles consist of hourly values averaged over one-year results. In this work, owners were assumed to connect their EVs when they arrive, assuming no limitations in available charging stations. On weekdays, people generally go to work in the morning and go back home in the evening, resulting in peaks of charging demand at those times. Since people generally do not work during weekends, the charging demand in office buildings showed no more peaks during the day.

The EV charging demand can affect the energy system significantly. The synchronism between EV charging behaviors and human presence can lead to aggregation of EV charging demand and appliance electricity demand, which will increase the peak-valley ratio of total electricity demand profiles. For residential-dominant neighborhoods, EV charging demand will increase the original evening peak as well as the peak-valley ratio. For office-dominant neighborhoods, EV charging demand will increase the ramping rate of electricity demand in the mornings, which will add new constraints to the energy system. Although the EV penetration in this work is low, it is worth noting that these adverse effects will be amplified as EV deployment increases. With regards to energy demand, the normalized EV charging demand is relatively small. However, with suitable management strategies, smart charging and vehicle-to-grid services can be used to shave peaks and fill the valley in a heat pump system and decouple electricity and heat generation in a CHP system to improve the penetration of renewable energy [65].

### *5.3. The influence of interconnectivity and the sector coupling*

The UCN introduces a modular architecture that facilitates scalability while interconnecting modules (cells). Three districts consisting of four (D-A), six (D-B), and nine (D-C) cells, respectively, were considered in this study to demonstrate the influence of interconnectivity by using the benchmark scenario ICI. Scenario D-A was taken into the discussion, as it comprises a simple architecture compared to D-B and D-C. Accordingly, two different architectures—UCN and IGS—were compared initially to evaluate the impact of the scalability introduced by the UCNs on the urban designing process.

The three Pareto fronts obtained using different techniques are presented in Fig. 12. A notable difference in NPV values and grid interactions can be observed when moving from UCN to ICI and FGS (refer to Table 2 for scenario definitions). A limited set of Pareto solutions were observed for FGS. The number of Pareto solutions increased when moving to ICI, and subsequently to UCN. Accordingly, the NPV reduced 7% and 30%, respectively, when moving from FGS to ICI and UCN. The results reveal that the interactions maintained between different cells help to improve the overall efficiency of the city when compared to sector coupling. However, a limited set of urban archetypes were considered in this study. A more comprehensive set of urban morphologies can easily increase the NPV gap between FGS and ICI. Even with the limited set of urban morphologies, the NPV gap reached over 37% (line BB in Fig. 12) when comparing FGS and UCN, which reveals the potential of the UCN to improve resource efficiency in cities while improving the interactions between different sectors and different parts of the city.

The changes in both urban morphology and the energy system design lead to a notable reduction in the overall investment. Further, it

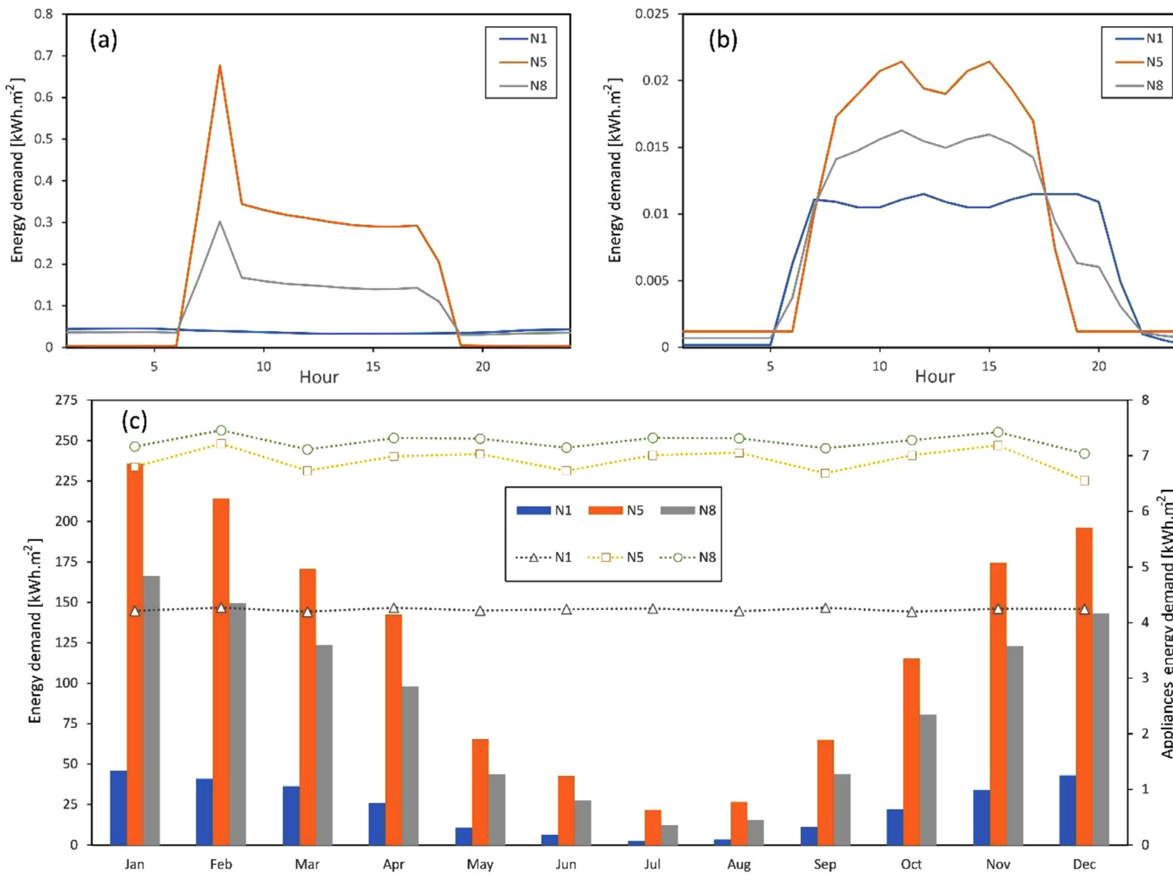


**Fig. 7.** Average demand per $m^2$ for three urban neighborhoods (N1, N5, N8): (a) average daily energy demand (a) average daily appliances energy demand (b) monthly energy and appliances demand.

facilitates the interactions among different sectors and localities. Three Pareto points (P, Q, and R in Fig. 12) were taken from the three Pareto fronts to analyze this further. P, Q, and R present the lowest cost designs for the FGS, ICI, and UCN scenarios. Urban morphologies obtained for these three scenarios are shown in Fig. 13(a). A clear change in urban morphology was observed when moving from UCN to FGS. The cells in UCN are entirely made out of Neighborhood-1 while the FGS is entirely made out of Neighborhood-9. ICI consists of two cells having Neighborhood-1 and the other two cells having Neighborhood 2. This reveals that considering sector coupling and interconnectivity among different urban cells has a notable impact on the urban morphology.

Similar to the urban morphology, connectivity between different sectors and different parts of the city can notably influence the energy system configuration and renewable energy integration. To further analyze this, ICI and UCN scenarios were further analyzed, taking Q and R design solutions. Renewable and dispatchable (non-renewable) energy capacities for the energy system installed in each cell are plotted in Fig. 13(b) (for R) and (c) (for Q). Furthermore, the ratio between installed renewable energy capacities to installed dispatchable energy capacities is presented in Fig. 13(d). A notable increase in the installed renewable energy capacity was observed when moving from Q (Fig. 13(c)) to R (Fig. 13(b)). More importantly, the ratio between renewable to dispatchable energy capacities installed often tends to be above one for the case of UCN (Fig. 13(d)), in contrast to ICI. In certain instances, such as in Cell 2 (Fig. 13(d)), the difference is quite significant. Considering all four systems, the renewable energy integration levels were 25% higher in UCN when compared to the ICI. This presents the potential of the UCN to improve sustainability in urban areas. Therefore, it can be concluded that UCN can improve urban sustainability levels while minimizing energy infrastructure costs. These unique features highlight the importance of moving into the UCN concept.

### 5.4. *Analyzing the influences due to interconnectivity at the cell level*

To analyze the impact of the interconnectivity at the cellular level, Pareto fronts were taken for both UCN and ICI scenarios (at cell level), as presented in Fig. 14. A notable reduction in the NPV and grid integration levels were observed in UCN when increasing the grid integration levels. This demonstrated that a significant reduction in NPV can be obtained for the UCN scenario, with a marginal allowance for grid integration. UCN uses a game-theoretic approach that enables stronger interactions among different cells, which helps to show the responses of different cells while proceeding with the overall optimization of the entire UCN. To better understand the phenomena, the evolution of the Pareto fronts for different iterations of UCN was taken, and they are presented in Fig. 14. The Pareto front obtained at the first iteration overlapped with the Pareto front of the ICI. A clear separation of the Pareto front was observed in the second iteration, where there was a clear split within the Pareto front. A sharp decrease in the NPV was observed up to a certain limit (Region N), and afterward, it followed the Pareto front obtained in ICI (Region M). However, after the third iteration onwards, the Pareto front looked quite similar to the final Pareto front (20th iteration). The deviation can be understood considering the grid curtailments. ICI does not consider the interactions between the cells, which often leads to peak generation during similar time intervals. As a result, the grid curtailments lead to introduce strict grid curtailments. UCN allows the interactions between the cells to be considered, reducing the grid curtailments by shifting the peak demands. As a result, a significant drop in the NPV is observed when increasing the grid integration lev-

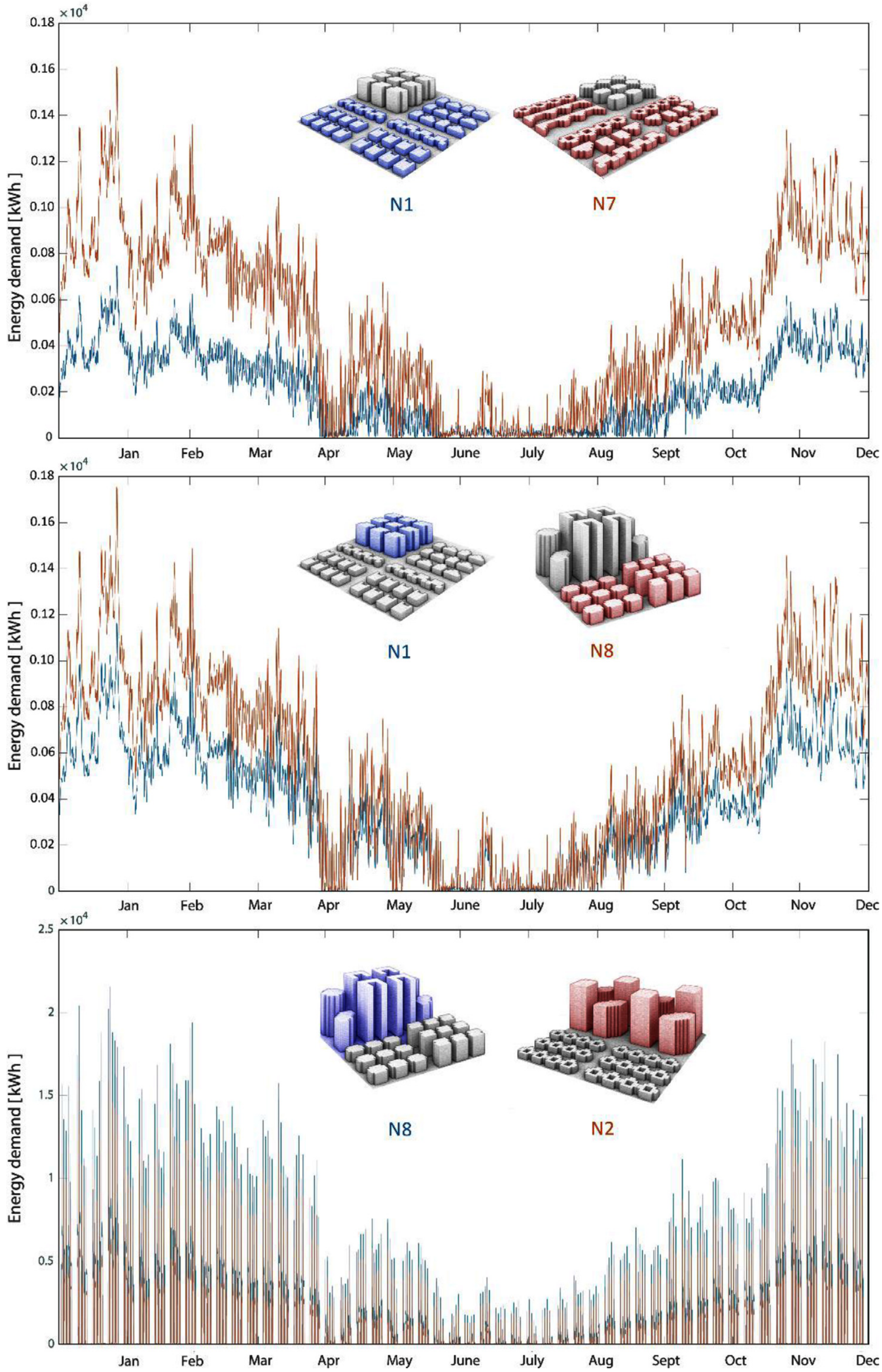


**Fig 8.** Hourly profiles of energy demand between neighborhoods with similar building types: Top: N1 and N7 (RE-SA), Middle: N1 and N8 (RE-MF), Bottom: N2 and N8 (OF-S).

els. This helps us to understand the cost reduction due to the iterative game-theoretical approach used in the UCN.

### 5.5. Advantage of the scalability

The modular approach of the urban cell concept enables several sectors to be integrated within a certain district, as well as to be connected with other local districts so they may interact. It is interesting to assess the scalability of the proposed approach (i.e., whether the proposed approach can be scaled up while maintaining the same level of leverage). D-C (nine cells) and D-B (six cells) scenarios were taken to further assist the analysis, along with the D-A (four cells), where each consists of four and nine cells, respectively. When analyzing the three scenarios it is prudent that a clear reduction in NPV beyond 25% is observed when using the UCN concept, irrespective of the number of cells considered, which clearly demonstrates the scalability of the proposed approach. The Pareto fronts obtained for the FGS scenario and ICI scenarios show a clear increase in the cost compared to the UCN, which can be presented as a vertical shift in the Pareto fronts as presented in Fig. 15 (a)

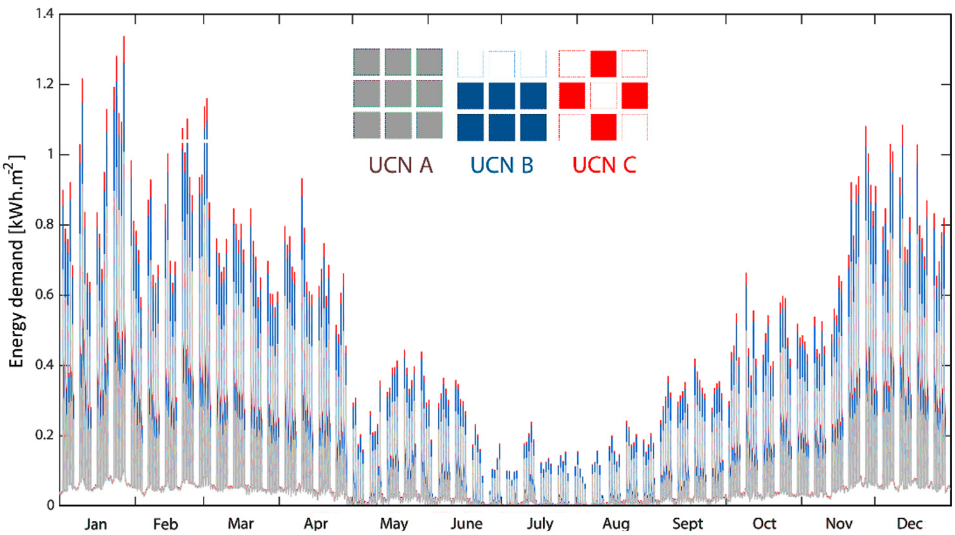


**Fig. 9.** Hourly profiles of energy demand per square meter for three urban cellular network scenarios: UCN A (considering nine neighborhoods), UCN B (considering six neighborhoods: N4, 5, 6, 7, 8, and 9), UCN C (considering four neighborhoods: N2, 4, 6, and 8).

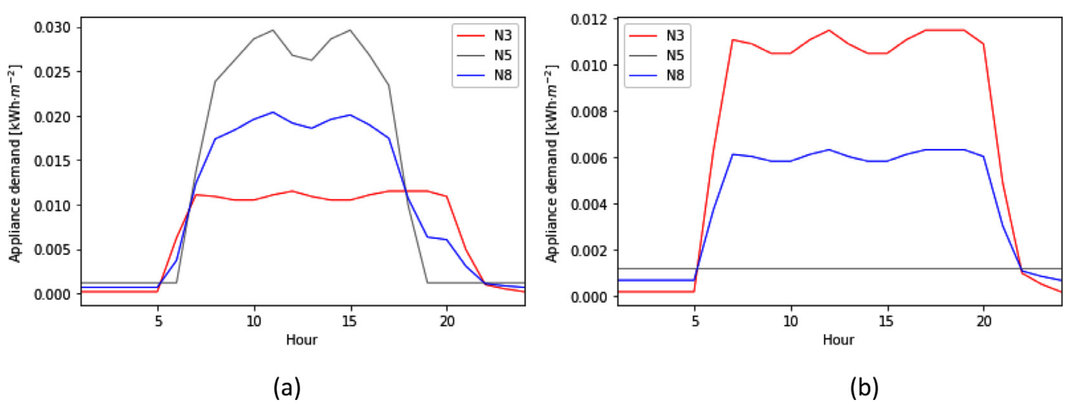


**Fig. 10.** Normalized electricity demand of appliance in different types of neighborhoods on (a) weekday and (b) weekend. N3: RE-SA and RE-MF, N5: OF-L, N8: OF-S and RE-MF.

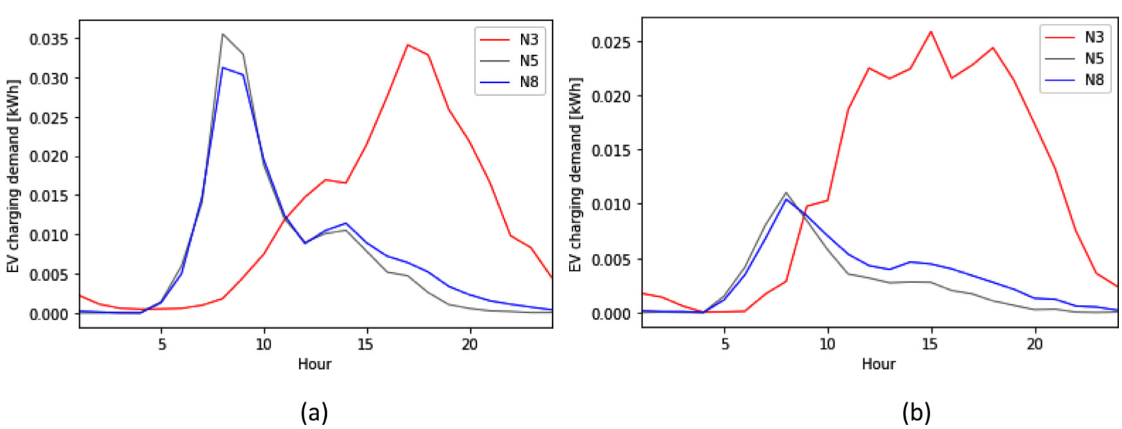


**Fig. 11.** Average EV charging demand for one EV in different types of neighborhoods on (a) weekday and (b) weekend.

(arrow I). The Pareto fronts tend to move both vertically and horizontally when moving D-B, as shown in Fig. 15 (b). When increasing the number of cells, the Pareto front shrank for both FGS and ICI. Although Pareto solutions were observed for minimal grid integration scenarios, the NPV did not reflect a significant reduction with the increase of grid integration level. When increasing the number of distributed energy systems without coordination, peak energy demands can easily coincide. As a result, notable investment is required on the network, which diminishes the advantage of connectivity. Therefore, the Pareto front shrank for both the FGS and ICI scenarios. When moving into D-C, the Pareto fronts for FGS and ICI became very short (consisting of just three and two solutions for ICI and FGS). Therefore, the Pareto front obtained after one game is presented as the ICI. These results indicate the importance of considering both sectors coupling and interconnectivity within cities. The proposed UCN concept facilitates both functions, which can notably improve resource efficiency within cities.

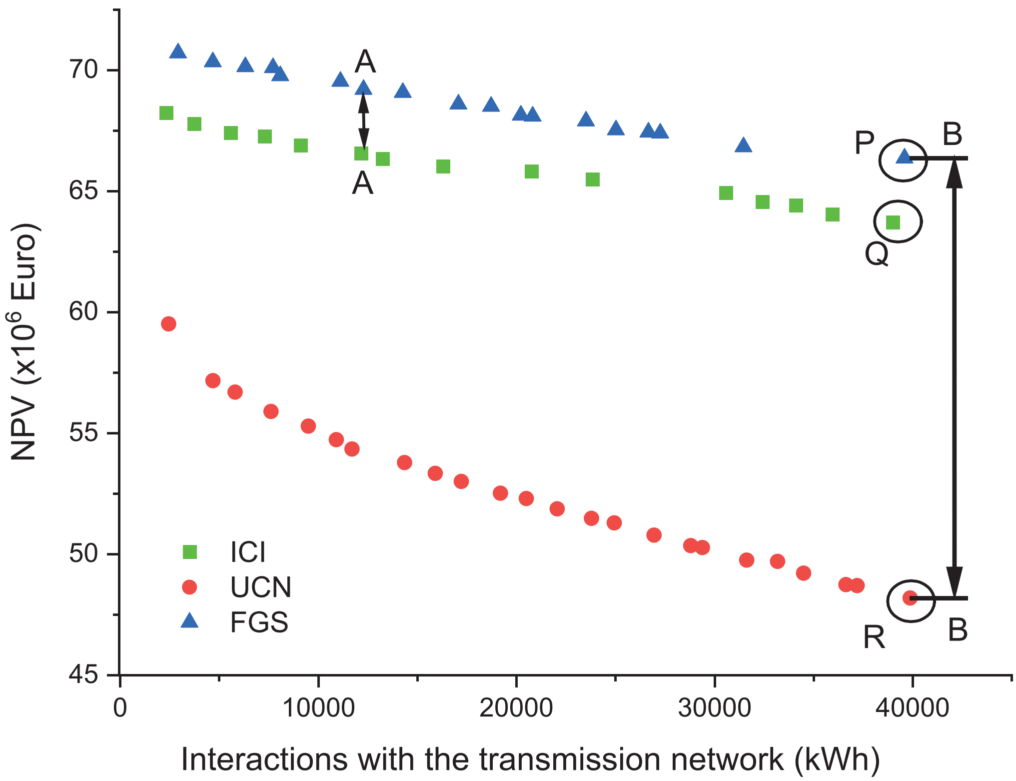


**Fig. 12.** Comparison of Pareto fronts obtained using the fixed generation scenario, isolated coupled infrastructure, and urban cellular network. P, Q, and R present the lowest NPV designs for the city concerning urban morphology and energy system design, respectively, for FGS, ICI, and UCN design approaches. The B-B link presents a 37% reduction in NPV.

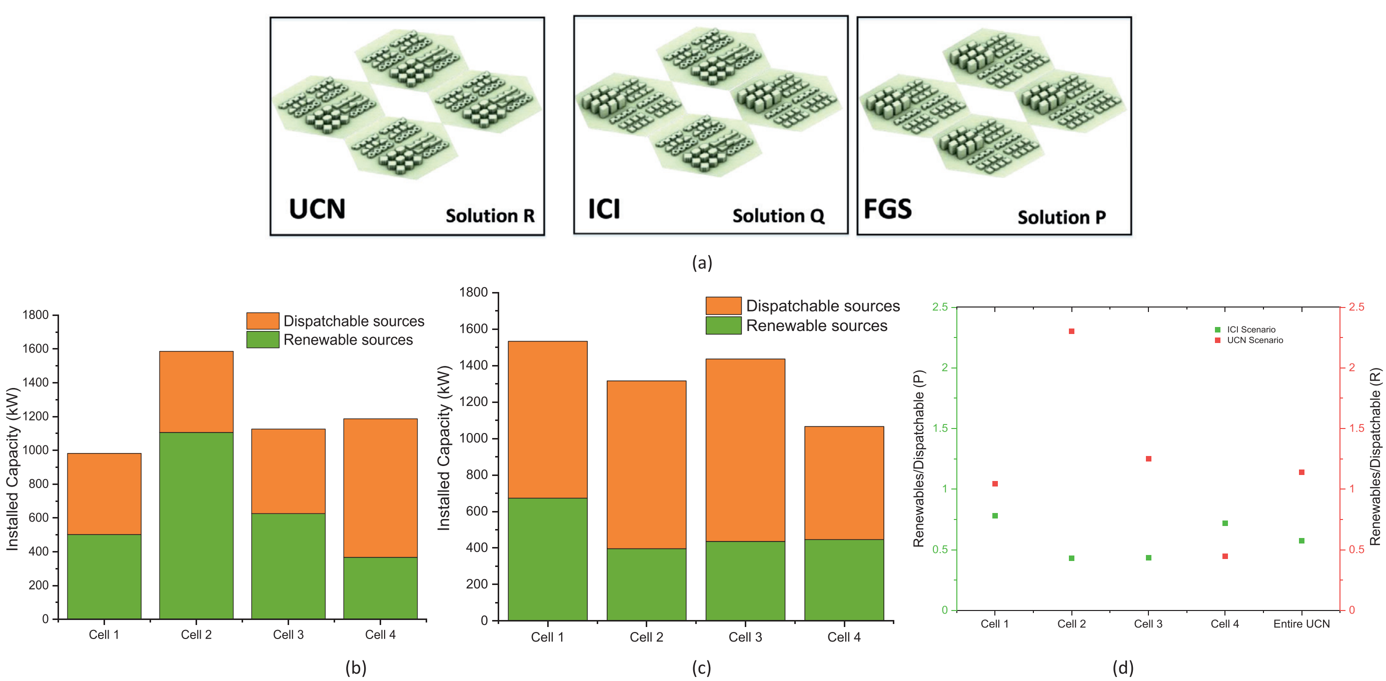


**Fig. 13.** The configuration of the solutions P, Q, and R. A notable change in urban morphology is observed when moving from P to Q and R, respectively, as shown in (a). The figure presents the urban morphology for the three solutions.

## 6. Conclusions

Cities grow at a rapid speed, bringing many challenges to urban planners. Often, urban areas have complex morphologies, which notably influence all the activities within the cities, including transportation and delivery of energy services. Considering these interactions among different sectors while accommodating complex urban morphology is usually discussed during the urban planning process. However, existing energy or urban concepts do not facilitate detailed consideration of interactions maintained within different sectors and parts of the cities, which

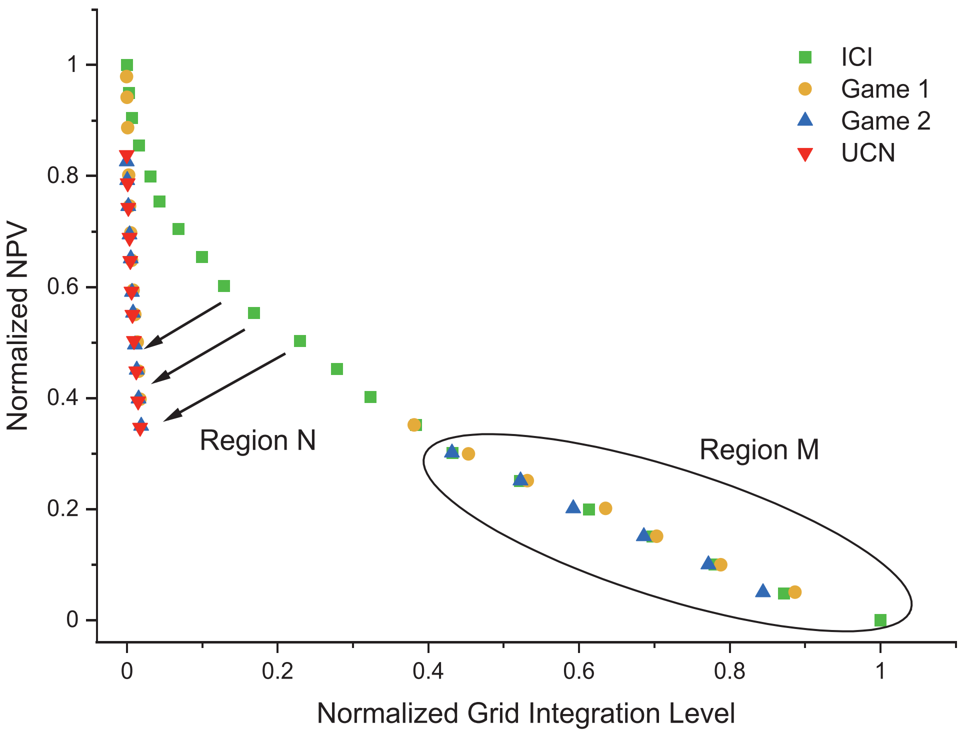


**Fig. 14.** Pareto fronts obtained for Cell 2. Game 1 and 2 represent the Pareto front obtained after two consecutive games, while the UCN presents the results after 20 games (Epsilon-Nash Equilibrium).

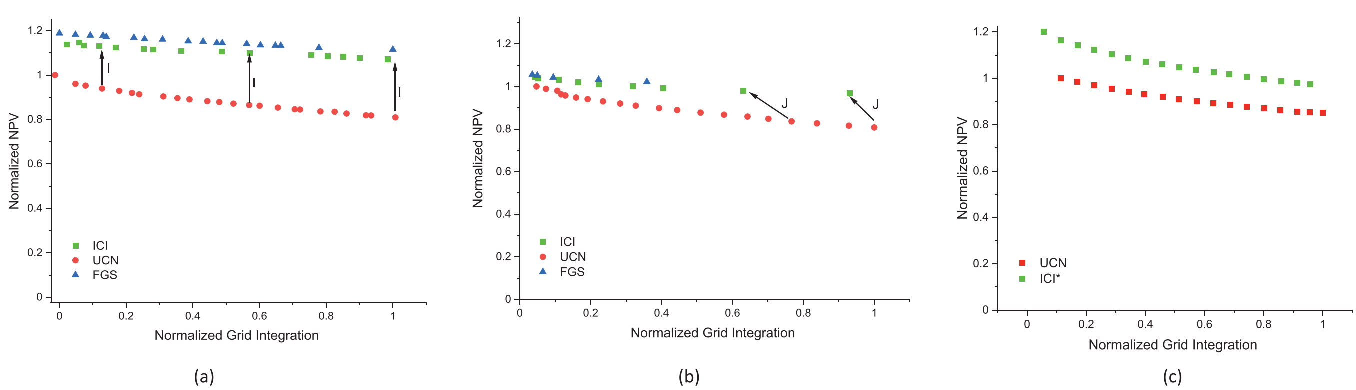


**Fig. 15.** Comparison of the Pareto fronts obtained for urban cellular networks having (a) four, (b) six, and (c) nine cells.

presents a major bottleneck in urban planning. Addressing this issue is vital to improving resource efficiency, autonomy, and sustainability of cities. The urban cell concept was introduced in this study to address these limitations in the present state of the art. The urban cell concept is a modular architecture where each cell represents an interconnected infrastructure that maintains energy interactions with another. Interactions between these modular units are maintained through a multiplex network. A game-theoretic approach can be used to maintain the interactions between the cells while preserving privacy.

Urban morphology at a modular cell can play a significant role when improving resource efficiency. Nine urban morphologies having different functional modes were taken and assessed for the urban morphology's influence on the energy demand. Subsequently, the energy demands for these different morphologies were simulated to understand the impact of urban morphology on energy demand. A notable difference in the annual energy demand and hourly energy demand pattern was observed when moving from one urban morphology to another. Similarly, the energy demand required for vehicle charging also showed a significant variation. Finally, the urban cell concept was used to optimize the urban morphology, energy system, and electricity network between the cells. The urban cell approach, which considers an efficient interactive methodology, was compared with the present state-of-the-art methods, taking Stockholm, Sweden, as the case study. The results revealed that the novel approach can reduce the net present value of the interconnected infrastructure by up to 37% through sector coupling and interconnectivity within the city. Irrespective of the number of cells considered, the difference in net present value between the urban cells and state-of-the-art approaches remained above 25%. This demonstrates the potential of the urban cell concept to improve resource efficiency in cities. Furthermore, the renewable penetration levels can be improved by 25% when using the urban cellular network concept. The urban cell concept can efficiently handle the complexity of the urban systems by facilitating sector coupling and interactions within the city while maintaining privacy, enabling the concept to be a game-changer in improving sustainability and resource efficiency in cities.

## Declaration of Competing Interest

None.

## References

[1] 68% of the world population projected to live in urban areas by 2050, says UN

| UN DESA | United Nations Department of Economic and Social Affairs 2018. https://www.un.org/development/desa/en/news/population/2018-revision-of-world-urbanization-prospects.html (accessed February 1, 2021).
[2] Lima I, Scalco V, Lamberts R. Estimating the impact of urban densification on high-rise office building cooling loads in a hot and humid climate. Energy Build 2019;182:30–44 https://doi.org/. doi:10.1016/j.enbuild.2018.10.019.
[3] Chokhachian A, Perini K, Giulini S, Auer T. Urban performance and density: generative study on interdependencies of urban form and environmental measures. Sustainable Cities and Society 2020;53:101952 https://doi.org/. doi:10.1016/j.scs.2019.101952.
[4] He B-J, Ding L, Prasad D. Relationships among local-scale urban morphology, urban ventilation, urban heat island and outdoor thermal comfort under sea breeze influence. Sustainable Cities and Society 2020;60:102289 https://doi.org/. doi:10.1016/j.scs.2020.102289.
[5] Zhang J, Xu L, Shabunko V, Tay SER, Sun H, Lau SSY, et al. Impact of urban block typology on building solar potential and energy use efficiency in tropical high-density city. Appl Energy 2019;240:513–33 https://doi.org/. doi:10.1016/j.apenergy.2019.02.033.
[6] Zhu R, Wong MS, You L, Santi P, Nichol J, Ho HC, et al. The effect of urban morphology on the solar capacity of three-dimensional cities. Renew Energy 2020;153:1111–26 https://doi.org/. doi:10.1016/j.renene.2020.02.050.
[7] Yu Z, Chen S, Wong NH. Temporal variation in the impact of urban morphology on outdoor air temperature in the tropics: a campus case study. Build Environ 2020;181:107132 https://doi.org/. doi:10.1016/j.buildenv.2020.107132.
[8] Mirzaee S, Özgun O, Ruth M, Binita KC. Neighborhood-scale sky view factor variations with building density and height: a simulation approach and case study of Boston. Urban Climate 2018;26:95–108 https://doi.org/. doi:10.1016/j.uclim.2018.08.012.
[9] Yuan C, Adelia AS, Mei S, He W, Li X-X, Norford L. Mitigating intensity of urban heat island by better understanding on urban morphology and anthropogenic heat dispersion. Build Environ 2020;176:106876 https://doi.org/. doi:10.1016/j.buildenv.2020.106876.
[10] Awol A, Bitsuamlak GT, Tariku F. Numerical estimation of the external convective heat transfer coefficient for buildings in an urban-like setting. Build Environ 2020;169:106557 https://doi.org/. doi:10.1016/j.buildenv.2019.106557.
[11] Sadeghi M, Wood G, Samali B, de Dear R. Effects of urban context on the indoor thermal comfort performance of windcatchers in a residential setting. Energy Build 2020;219:110010 https://doi.org/. doi:10.1016/j.enbuild.2020.110010.
[12] Javanroodi K, Nik VM. Impacts of Microclimate Conditions on the Energy Performance of Buildings in Urban Areas. Buildings 2019;9:189 https://doi.org/. doi:10.3390/buildings9080189.
[13] Chen H-C, Han Q, De Vries B. Modeling the spatial relation between urban morphology, land surface temperature and urban energy demand. Sustainable Cities and Society 2020;60:102246 https://doi.org/. doi:10.1016/j.scs.2020.102246.
[14] Nasrollahi N, Shokri E. Daylight illuminance in urban environments for visual comfort and energy performance. Renewable Sustainable Energy Rev 2016;66:861–74 https://doi.org/. doi:10.1016/j.rser.2016.08.052.
[15] Perera ATD, Coccolo S, Scartezzini J-L. The influence of urban form on the grid integration of renewable energy technologies and distributed energy systems. Sci Rep 2019;9:1–14 https://doi.org/. doi:10.1038/s41598-019-53653-w.
[16] Perera ATD, Javanroodi K, Nik VM. Climate resilient interconnected infrastructure: co-optimization of energy systems and urban morphology. Appl Energy 2021;285 https://doi.org/. doi:10.1016/j.apenergy.2020.116430.
[17] Shortt A, O'Malley M. Quantifying the Long-Term Impact of Electric Vehicles on the Generation Portfolio. IEEE Trans Smart Grid 2014;5:71–83 https://doi.org/. doi:10.1109/TSG.2013.2286353.
[18] Asarpota K, Nadin V. Energy Strategies, the Urban Dimension, and Spatial Planning. Energies 2020;13:3642 https://doi.org/. doi:10.3390/en13143642.
[19] Xu Y, Çolak S, Kara EC, Moura SJ, González MC. Planning for electric vehicle needs by coupling charging profiles with urban mobility. Nature Energy 2018;3:484–93 https://doi.org/. doi:10.1038/s41560-018-0136-x.
[20] Farhangi H. The path of the smart grid. IEEE Power Energ Mag 2010;8:18–28 https://doi.org/. doi:10.1109/MPE.2009.934876.
[21] Buffa S, Cozzini M, D'Antoni M, Baratieri M, Fedrizzi R. 5th generation district heating and cooling systems: a review of existing cases in. Europe. Renewable and Sustainable Energy Reviews 2019;104:504–22 https://doi.org/. doi:10.1016/j.rser.2018.12.059.
[22] Perera ATD, Madusanka AN, Attalage RA, Perera KKCK. A multi criterion analysis for renewable energy integration process of a standalone hybrid energy system with internal combustion generator. J Renewable Sustainable Energy 2015;7:043128 https://doi.org/. doi:10.1063/1.4928684.
[23] Geidl M, Koeppel G, Favre-Perrod P, Klockl B, Andersson G, Frohlich K. Energy hubs for the future. IEEE Power Energ Mag 2007;5:24–30 https://doi.org/. doi:10.1109/MPAE.2007.264850.
[24] Perera ATD, Wang Z, Nik VM, Scartezzini J-L. Towards realization of an Energy Internet: designing distributed energy systems using game-theoretic approach. Appl Energy 2021;283:116349 https://doi.org/. doi:10.1016/j.apenergy.2020.116349.
[25] Wang Z, Perera ATD. Integrated platform to design robust energy internet. Appl Energy 2020;269:114942 https://doi.org/. doi:10.1016/j.apenergy.2020.114942.
[26] Buttler A, Spliethoff H. Current status of water electrolysis for energy storage, grid balancing and sector coupling via power-to-gas and power-to-liquids: a review. Renewable Sustainable Energy Rev 2018;82:2440–54 https://doi.org/. doi:10.1016/j.rser.2017.09.003.
[27] Cao J, Crozier C, McCulloch M, Fan Z. Optimal Design and Operation of a Low Carbon Community Based Multi-Energy Systems Considering EV Integration. IEEE Trans Sustainable Energy 2019;10:1217–26 https://doi.org/. doi:10.1109/TSTE.2018.2864123.
[28] Murray P, Carmeliet J, Orehounig K. Multi-Objective Optimisation of Power-to-Mobility in Decentralised Multi-Energy Systems. Energy 2020;205:117792 https://doi.org/. doi:10.1016/j.energy.2020.117792.
[29] Murray P, Orehounig K, Carmeliet J. Optimal vehicle selection in the design of urban energy systems: an integration of the private transport and building energy sectors. Rome, Italy: Nd; 2019.
[30] Lam AYS, Leung Y-W, Chu X. Electric Vehicle Charging Station Placement: formulation, Complexity, and Solutions. IEEE Trans Smart Grid 2014;5:2846–56 https://doi.org/. doi:10.1109/TSG.2014.2344684.
[31] Perera ATD, Coccolo S, Scartezzini J-L, Mauree D. Quantifying the impact of urban climate by extending the boundaries of urban energy system modeling. Appl Energy 2018;222:847–60 https://doi.org/. doi:10.1016/j.apenergy.2018.04.004.
[32] Perera ATD, Coccolo S, Scartezzini J-L. The influence of urban form on the grid integration of renewable energy technologies and distributed energy systems. Sci Rep 2019;9:17756 https://doi.org/. doi:10.1038/s41598-019-53653-w.
[33] Mohajeri N, Perera ATD, Coccolo S, Mosca L, Le Guen M, Scartezzini J-L. Integrating urban form and distributed energy systems: assessment of sustainable development scenarios for a Swiss village to 2050. Renew Energy 2019;143:810–26 https://doi.org/. doi:10.1016/j.renene.2019.05.033.
[34] Perera ATD, Kamalaruban P. Applications of reinforcement learning in energy systems. Renewable Sustainable Energy Rev 2021;137:110618 https://doi.org/. doi:10.1016/j.rser.2020.110618.
[35] Poon KH, Kämpf JH, Tay SER, Wong NH, Reindl TG. Parametric study of URBAN morphology on building solar energy potential in Singapore context. Urban Climate 2020;33:100624 https://doi.org/. doi:10.1016/j.uclim.2020.100624.
[36] Xu X, AzariJafari H, Gregory J, Norford L, Kirchain R. An integrated model for quantifying the impacts of pavement albedo and urban morphology on building energy demand. Energy Build 2020;211:109759 https://doi.org/. doi:10.1016/j.enbuild.2020.109759.
[37] Oh M, Kim Y. Identifying urban geometric types as energy performance patterns. Energy for Sustainable Development 2019;48:115–29 https://doi.org/. doi:10.1016/j.esd.2018.12.002.
[38] Javanroodi K, Nik VM, Yang Y. Optimization of building form and its fenestration in response to microclimate conditions of an urban area. E3S Web of Conferences 2020;172 Article number: 19002.
[39] Martins TA de L, Faraut S, Adolphe L. Influence of context-sensitive urban and architectural design factors on the energy demand of buildings in Toulouse. France. Energy and Buildings 2019;190:262–78 https://doi.org/. doi:10.1016/j.enbuild.2019.02.019.
[40] Rodríguez-Álvarez J. Urban Energy Index for Buildings (UEIB): a new method to evaluate the effect of urban form on buildings' energy demand. Landsc Urban Plan 2016;148:170–87 https://doi.org/. doi:10.1016/j.landurbplan.2016.01.001.
[41] Javanroodi K. Wind-phil architecture: optimization of high-rise buildings form for efficient summer cooling in tehran. Tehran: Tarbiat Modares University; 2018.
[42] Javanroodi K, Mahdavinejad M, Nik VM. Impacts of urban morphology on reducing cooling load and increasing ventilation potential in hot-arid climate. Appl Energy 2018;231:714–46 https://doi.org/. doi:10.1016/j.apenergy.2018.09.116.
[43] Ladybug Tools | Dragonfly n.d. https://www.ladybug.tools/dragonfly.html (accessed September 30, 2020).
[44] Javanroodi K, Nik VM, Mahdavinejad M. A novel design-based optimization framework for enhancing the energy efficiency of high-rise office buildings in urban areas. Sustainable Cities and Society 2019;49:101597 https://doi.org/. doi:10.1016/j.scs.2019.101597.
[45] Javanroodi K, Nik VM. Interactions between extreme climate and urban morphology: investigating the evolution of extreme wind speeds from mesoscale to microscale. Urban Climate 2020;31:100544 https://doi.org/. doi:10.1016/j.uclim.2019.100544.
[46] Johansson S, Persson J, Lazarou S, Theocharis A. Investigation of the Impact of Large-Scale Integration of Electric Vehicles for a Swedish Distribution Network. Energies 2019;12:4717 https://doi.org/. doi:10.3390/en12244717.
[47] Smart J, Schey S. Battery Electric Vehicle Driving and Charging Behavior Observed Early in The EV Project. SAE International Journal of Alternative Powertrains 2012;1:27–33.
[48] Durisch W, Bitnar B, Mayor J-C, Kiess H, Lam K, Close J. Efficiency model for photovoltaic modules and demonstration of its application to energy yield estimation. Sol Energy Mater Sol Cells 2007;91:79–84 https://doi.org/. doi:10.1016/j.solmat.2006.05.011.
[49] Perera ATD, Wickramasinghe PU, Nik VM, Scartezzini J-L. Introducing reinforcement learning to the energy system design process. Appl Energy 2020;262:114580 https://doi.org/. doi:10.1016/j.apenergy.2020.114580.
[50] Perera ATD, Nik VM, Mauree D, Scartezzini J-L. An integrated approach to design site specific distributed electrical hubs combining optimization, multi-criterion assessment and decision making. Energy 2017;134:103–20 https://doi.org/. doi:10.1016/j.energy.2017.06.002.
[51] Perera ATD, Nik VM, Mauree D, Scartezzini J-L. Electrical hubs: an effective way to integrate non-dispatchable renewable energy sources with minimum impact to the grid. Appl Energy 2017;190:232–48 https://doi.org/. doi:10.1016/j.apenergy.2016.12.127.
[52] Deb K, Mohan M, Mishra S. Evaluating the $\epsilon$-Domination Based Multi-Objective Evolutionary Algorithm for a Quick Computation of Pareto-Optimal Solutions. Evol Comput 2005;13:501–25 https://doi.org/. doi:10.1162/106365605774666895.
[53] Perera ATD. Modeling and Assessment of Urban Energy Systems. Infoscience 2019 https://doi.org/. doi:10.5075/epfl-thesis-9389.

[54] Romero R, Monticelli A, Garcia A, Haffner S. Test systems and mathematical models for transmission network expansion planning. Transmission and Distribution IEE Proceedings - Generation 2002;149:27–36 https://doi.org/. doi:10.1049/ip-gtd:20020026.
[55] Nielsen MM. Remote sensing for urban planning and management: the use of window-independent context segmentation to extract urban features in Stockholm. Comput Environ Urban Syst 2015;52:1–9 https://doi.org/. doi:10.1016/j.compenvurbsys.2015.02.002.
[56] Sweden's National Report for the third United Nations Conference on Housing and Sustainable Urban Development (Habitat III). Swedish National Report; n.d.
[57] ud software development | urban microclimate n.d. https://urbanmicroclimate.scripts.mit.edu/umc.php (accessed September 30, 2020).
[58] Abohela I, Hamza N, Dudek S. Effect of roof shape, wind direction, building height and urban configuration on the energy yield and positioning of roof mounted wind turbines. Renew Energy 2013;50:1106–18 https://doi.org/. doi:10.1016/j.renene.2012.08.068.
[59] Mahdavinejad M, Javanroodi K. Impact of roof shape on air pressure, wind flow and indoor temperature of residential buildings. Null 2016;7:87–103 https://doi.org/. doi:10.1080/2093761X.2016.1167645.
[60] De Jaeger I, Reynders G, Ma Y, Saelens D. Impact of building geometry description within district energy simulations. Energy 2018;158:1060–9 https://doi.org/. doi:10.1016/j.energy.2018.06.098.
[61] Number of registered passenger cars in Sweden from 1990 to 2017. Statista 2019. https://www.statista.com/statistics/452397/sweden-number-of-registered-passenger-cars/.
[62] Trafik analys. Mileage report for Swedish registered vehicle 2019. https://www.trafa.se/globalassets/statistik/vagtrafik/korstrackor/2020/korstrackor_2019.pdf. Last accessed:2020.06.05.
[63] ROSSBACH K. Analysis of future scenarios for electric vehicle adoption in sweden. Master MDH; 2015.
[64] Lin H, Fu K, Wang Y, Sun Q, Li H, Hu Y, et al. Characteristics of electric vehicle charging demand at multiple types of location - Application of an agent-based trip chain model. Energy 2019;188:116122 https://doi.org/. doi:10.1016/j.energy.2019.116122.
[65] Wang Y, Mauree D, Sun Q, Lin H, Scartezzini JL, Wennersten R. A review of approaches to low-carbon transition of high-rise residential buildings in China. Renewable Sustainable Energy Rev 2020;131:109990 https://doi.org/. doi:10.1016/j.rser.2020.109990.